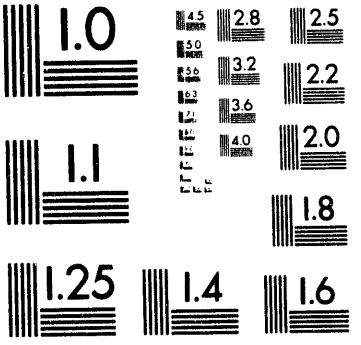
1.0
4.5
2.8
2.5
5.0
3.2
2.2
5.6
3.6
2.0
6.3
4.0
1.1
1.8
1.25
1.4
1.6

1 of 1

T9398 (2)

PREPARED FOR THE U.S. DEPARTMENT OF ENERGY,
UNDER CONTRACT DE-AC02-76-CHO-3073

PPPL-2898
UC-420,426

PPPL-2898

STUDIES OF LOCAL ELECTRON HEAT TRANSPORT ON TFTR

BY

E.D. FREDRICKSON, Z. Y. CHANG, A. JANOS, ET AL.

AUGUST, 1993

PRINCETON
PLASMA PHYSICS
LABORATORY

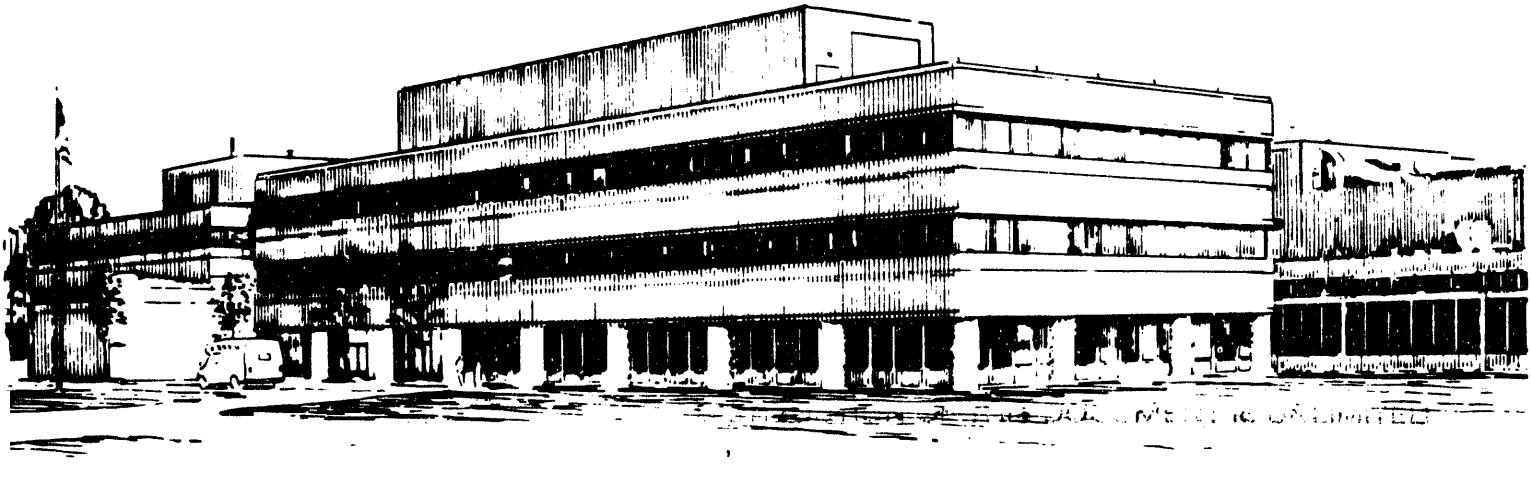

NOTICE

This report was prepared as an account of work sponsored by an agency of the United States Government. Neither the United States Government nor any agency thereof, nor any of their employees, makes any warranty, express or implied, or assumes any legal liability or responsibility for the accuracy, completeness, or usefulness of any information, apparatus, product, or process disclosed, or represents that its use would not infringe privately owned rights. Reference herein to any specific commercial produce, process, or service by trade name, trademark, manufacturer, or otherwise, does not necessarily constitute or imply its endorsement, recommendation, or favoring by the United States Government or any agency thereof. The views and opinions of authors expressed herein do not necessarily state or reflect those of the United States Government or any agency thereof.

NOTICE

This report has been reproduced from the best available copy.
Available in paper copy and microfiche.

Number of pages in this report: 53

DOE and DOE contractors can obtain copies of this report from:

Office of Scientific and Technical Information
P.O. Box 62
Oak Ridge, TN 37831;
(615) 576-8401.

This report is publicly available from the:

National Technical Information Service
Department of Commerce
5285 Port Royal Road
Springfield, Virginia 22161
(703) 487-4650

August 16, 1993

Studies of Local Electron Heat Transport on TFTR

E. D. Fredrickson, Z. Y. Chang, A. Janos,
K. M. McGuire, S. Scott, and G. Taylor
Princeton Plasma Physics Laboratory
Princeton, NJ 08543

Abstract

The anomalously fast relaxation of the perturbations to the electron temperature profile caused by a sawtooth crash has been studied extensively on TFTR. We will show that on a short timescale the heat pulse is not simply diffusive as has been generally assumed, but that modeling of the heat pulse requires a transient enhancement in χ_e following the sawtooth crash. It will be shown that the time-dependent enhancement in χ_e predicted by non-linear thermal transport models, *i.e.*, incremental χ models or the Rebut-Lallia-Watkins transport model, is much smaller than that required to explain the anomalies in the heat pulse propagation.

MASTER

Introduction

The transport of thermal energy in tokamak plasmas has long been known to be larger than neoclassical calculations predict. It is commonly assumed that 'small' scale electrostatic turbulence, magnetic stochasticity or some similar mechanism is responsible for the enhanced transport.[1] Studies of the propagation of heat pulses following sawtooth crashes started with the hope that this approach would yield a local measurement of the electron thermal diffusivity, independent of the uncertainties of power balance analysis, and which then might improve understanding of the nature of anomalous transport.[2,3]

When studies of sawtooth induced heat pulse propagation were undertaken on TFTR,[4] it was found that the heat pulse propagation was not consistent with the estimates of thermal diffusivity, χ_e from power balance analysis. These results suggested several interesting possible explanations, including that the model of the sawtooth crash was incomplete or that the heat flux had a non-linear dependence on the temperature gradient.[4,5] Recently there has been renewed interest in both of these possibilities. New experimental and theoretical evidence suggests that the sawtooth crash mechanism may transiently enhance the electron thermal conductivity in the region outside the mixing radius.[6] The interest in 'incremental' or nonlinear models for χ_e is motivated in part by the long standing observation of the 'resilience' of the electron temperature profile to changes in the heating profile[7-10] and more recently by JET results which have purported to find agreement between the electron thermal diffusivity determined from heat pulse analysis, χ^{HP}, and the χ^{inc} determined from power balance analysis of parameter scans.[11] However, in this paper it will be shown that χ^{HP} is several times larger than the χ^{inc} for TFTR data.

In this paper we will demonstrate that it is not possible, at least for TFTR data, to simulate the sawtooth induced heat pulses with a simple model for heat diffusion, thus χ^{HP} derived from sawtooth induced heat pulses is not a meaningful quantity. At small minor radii, in the radial range $r_{mix} < r < 1.4r_{mix}$, the heat pulse propagation can be dominated by the ballistic effect.[6] (Throughout this paper, r_{mix} will have the standard definition, *i.e.*, the radius to which the sawtooth crash flattens the temperature profile.) At larger minor radius (later times) the ratio of signal-to-noise is lower and

the sharp features present at smaller radii (shorter timescales) have largely relaxed with the result that the heat pulse shapes may be approximately simulated with many models, e.g., the options of varying the radial profile of χ^{inc} or χ, introducing coupling to the density pulse[12] or including an anomalous damping term[13] allow considerable leeway for approximate fits to the experimental data. Thus, at neither small nor large minor radius is it possible to draw unambiguous conclusions about the nature of anomalous transport for sawtooth induced heat pulse studies.

In the first part of this paper we will discuss the limitations inherent in comparing diffusion coefficients inferred from global power balance (χ^{PB}) to those inferred from the change in the temperature gradient induced by increasing the heat flux (χ^{inc}) or those inferred from analysis of heat pulses from sawtooth crashes (χ^{HP}). In the second section experimental data on sawtooth induced heat pulse propagation will be presented, beginning with studies of the heat pulse propagation on a fast time scale following the sawtooth crash, followed by studies of the scaling of χ^{HP}. (In this paper, all heat pulses discussed are induced by sawteeth and the qualifier will be dropped for brevity.) In the third section numerical simulations of the electron temperature profile evolution following a sawtooth crash are performed to investigate the relationship between the power balance studies and the heat pulse propagation studies. The simulations use either an explicit time and space dependent χ_e, or various non-linear models for χ_e, to provide the necessary time dependence. The experimental data are from neutral beam heated plasmas in TFTR with $I_P \leq 1.9$ MA, $P_{beam} \leq 30$ MW, $a_P = 0.8 - 0.9$ m, and $B_{tor} = 4 - 5$ Tesla.

The original studies of heat pulses on ORMAC, ISX-B, TFTR and elsewhere relied primarily on soft x-ray cameras, with the concomitant problems of chord averaging and lack of amplitude information.[2,4,14] Many more recent heat pulse propagation studies have used relatively fast measurements of the electron cyclotron emission from which a local electron temperature is inferred.[5,13,15] For the present studies, the principal diagnostic is the fast (200 kHz bandwidth) grating polychromator (GPC) which measures the electron cyclotron emission (ECE) intensity, providing a 20 point temperature profile with a channel spacing of about 6 cm and a radial spatial resolution of about 3 cm. The GPC is not absolutely calibrated and thus must be cross-calibrated to another of the electron temperature profile diagnostics (i.e., the Thomson

scattering system, the ECE radiometer or Michelson interferometer). The ability to make fast (200kHz), absolute measurements of the electron temperature profile is essential for study of the heat pulse propagation in the region $r_{mix} < r < 1.4r_{mix}$, the region where the ballistic response dominates. The use of local T_e measurements allows direct measurement of the mixing radius for the sawtooth crash and the radial dependence of the heat pulse amplitude.

The ECE temperature diagnostics give measurements of the electron temperature profile as a function of frequency. Those frequencies must be mapped to spatial locations through a calculation of the magnetic field. For the data presented in this paper, the mapping is done using data from the SNAP code which calculates the paramagnetic, diamagnetic and poloidal field corrections to the vacuum toroidal magnetic field. The measurements are then mapped to the flux surface averaged minor radius using the SNAP calculation of the Shafranov shift. This mapping will not change significantly [due to changes in $J(r)$ or plasma pressure] during the sawtooth crash.

I. Determination of χ^{inc}

Studies of the dependence of the *total* heat flux, Q_{tot}, on $n\nabla T$ carried out on the JET tokamak have found that the 1-fluid incremental-χ, χ_{1f}^{inc}, as measured from such a heat flux analysis of temperature scans is similar to the χ^{HP} (the 1-fluid χ_{1f}^{inc} is an effective diffusivity where the heat flow through the ion and electron channels is not separated). This result suggested a common origin for the observed non-linear (offset linear) dependence of the heat flux on $n_e\nabla T_e$ and the fast heat pulse propagation (where $\nabla T = \partial T/\partial r$). A model was proposed for which $\chi^{HP} = \chi_e^{inc} \geq \chi_e^{PB}$, and it was claimed that in general, χ^{HP} should equal χ^{inc}. However, the χ^{HP} should be compared to χ_e^{PB} or χ_e^{inc}, not χ_{1f}^{inc}. For example, the χ_{1f}^{PB} could deviate systematically from the χ_e^{PB} due to systematic changes in the electron-ion heat transfer, resulting in large differences between the inferred χ_e^{inc} and χ_{1f}^{inc}. In this section we will show with data from TFTR that the experimentally determined incremental electron thermal diffusivity, χ_e^{inc}, is not equal to the experimental χ^{HP}. We will further demonstrate theoretically that only under the condition that Q_e depends only on ∇T_e (and not T_e), does $\chi^{HP} = \chi^{inc}$.

A measure of the incremental *electron* thermal diffusivity was obtained

on TFTR by making a scan of the electron temperature at constant electron density. This was accomplished by increasing the beam power and decreasing the gas feed to compensate for the increased fueling from the beams. A power balance analysis of the data from these scans was done using the SNAP time-independent analysis code where the power flow through the electron and ion channels was calculated separately. Measurements of the electron temperature, ion temperature, and electron density profiles were used in the analysis.

In Fig. 1 the total heat flux through the electrons for the different shots in this scan is graphed against the local $n_e \nabla T_e$ for three minor radii. Included in this scan is a shot at somewhat higher beam power for which extensive heat pulse analysis will be performed. Also included for completeness (the open symbols) is the data from an ohmic shot at the same density, but for which ion temperature profiles could not be measured. For these shots the power balance transport analysis code assumes $\chi_i = \chi_e$ and performs a series of iterations to determine the ion temperature. The points representing the beam heated data (solid symbols) show a non-linear dependence of Q_e on either T_e or ∇T_e, however, it is difficult to distinguish experimentally between an offset linear fit to the data (if the ohmic points are eliminated) implying a model with a fixed incremental χ, or a parabolic fit implying $\chi_e \propto T_e$ or ∇T_e. However, for the highest power point, the χ_e^{inc} is approximately twice χ_e^{PB} at all radii. It has been previously shown that $\chi^{HP} \approx 5\chi^{PB}$ for this point.[6] These results are not consistent with an incremental χ model.[5] While a more general treatment of the dependence of thermal diffusivity on local parameters can reconcile the observation that $\chi^{HP} \approx 2.5\chi^{inc}$ as will be demonstrated in the remainder of this section, a more detailed study of the heat pulse shapes in the following sections strongly suggests that the bulk of the sawtooth induced heat pulse propagation anomaly results from the physics of the sawtooth crash itself.

The above results demonstrate that experimentally χ^{HP}, which applies to small perturbations about the equilibrium profile, and χ^{inc} which applies to incremental changes in the equilibrium profile may be very different. The distinction is also necessary when considering non-linear models for χ_e which have a dependence on T_e (or the temperature gradient scale length $L_T \equiv T_e/\nabla T_e$) as well as ∇T_e.[16] The effect of this 'scale length' term in equilibrium studies is negligible; in equilibrium the shape of the temperature

profile does not change significantly,[7-10] *i.e.*, as $T_e \propto \nabla T_e$. Conversely, in perturbation studies the relative change in T_e is much less than the change in ∇T_e, making the dependence on the temperature gradient scale length important and the dependence on T_e unimportant. In the following discussions it will be assumed that the electron temperature profile is 'resilient'.[7]

An expression for the effective perturbative thermal diffusivity, χ^{HP}, can be determined by linearizing the thermal transport equation with $\chi = \chi(\nabla T)$

$$\frac{3n}{2}\frac{\partial T}{\partial t} = \frac{1}{r}\frac{\partial}{\partial r} rn\chi(\nabla T)\frac{\partial T}{\partial r} + Q \tag{1}$$

to get an equation describing the evolution of the perturbed temperature,[4] $\tilde{T} \equiv T(t) - < T(t) >_{time}$,

$$\frac{3n}{2}\frac{\partial \tilde{T}}{\partial t} = \frac{1}{r}\frac{\partial}{\partial r} rn\chi^{HP}\frac{\partial \tilde{T}}{\partial r} \tag{2}$$

where the

$$\chi^{HP} \equiv \left[\frac{\partial[\nabla T\chi(\nabla T)]}{\partial[\nabla T]}\right]_{\nabla T = \nabla T_o}. \tag{3}$$

Thus the effective χ describing the relaxation of perturbations to the temperature is χ^{HP}. In this exercise perturbations in the radiative cooling, electron-ion coupling and heating terms were neglected. These terms introduce an effective damping of the heat pulse, however the time-constant for TFTR plasmas is much longer ($\approx$ 100msec) than the pulse propagation time, and thus may be ignored.

The *incremental* χ is determined by making small changes in the *equilibrium* plasma temperature and measuring the resulting change in equilibrium thermal transport. For example, transport analysis of data from T_e scans, *e.g.*, produced by increasing the neutral beam power at constant density, show (c.f. Fig. 1) that the heat flux is not a linear function of $n_e\nabla T_e$. An incremental (for added power input) thermal diffusivity is defined as the local slope of Q_e versus $n_e\nabla T_e$, *i.e.*,

$$\chi_e^{inc} \equiv \delta(Q_e)/\delta_e(n\nabla T_e). \tag{4}$$

As these are studies of equilibrium plasma parameters, the decoupling of temperature and temperature gradient present in the perturbative studies is

not present. As a manifestation of the electron temperature profile resiliency observed on TFTR and other machines, both T_e and ∇T_e are changing proportionally; a dependence of χ on T will affect the transport in the same manner as a similar dependence on ∇T_e. Thus, while the definitions of χ^{HP} and χ^{inc} appear superficially similar, they are in general very different.

Three models are considered to illustrate the inherent difference between the χ^{HP} and χ^{inc}. The first model, the incremental χ model, is the simplest and is advertised as a general linearization of non-linear transport models. The second is a model commonly used in machine design studies, the Rebut-Lallia-Watkins (RLW) transport model.[17] The third is a generic power-law model of the form, $\chi \propto T_e^{\alpha} L_T^{-\beta}$ which is introduced to illustrate in general how differences in χ^{HP} and χ^{inc} can be resolved.

The incremental χ model in its simplest form is

$$\chi(r,t) = \chi^{inc}(1 - \nabla T_{crit}/\nabla T) \tag{5}$$

where ∇T_{crit} represents the critical temperature gradient at which some, unspecified, instability begins to dominate the transport. Here it will be assumed that ∇T_{crit} and χ^{inc} are constants; in practice, of course, both parameters can have radial dependencies and some additional parameters must be introduced to deal with regions where $\nabla T < \nabla T_{crit}$. However, outside the mixing radius for sawtooth heat pulses, this model predicts that $\chi^{HP} = \chi^{inc}$.[11] For the data in Fig. 1, the highest power point has $\nabla T \approx 2\nabla T_{crit}$, thus the incremental-$\chi$ model would predict that $\chi^{HP} \approx 2\chi^{PB}$. A factor of five is observed experimentally.

The RLW model is superficially similar to the incremental χ model, but as will be seen the differences are significant. The relevant form of the RLW model for perturbative and incremental transport studies is

$$\chi = \chi_{an}^{rlw}[1 - \nabla T_{crit}^{rlw}/\nabla T]. \tag{6}$$

The coefficients χ_{an}^{rlw} and ∇T_{crit}^{rlw} are not constant but depend on local plasma parameters,[17] including a dependence on the temperature gradient scale length, L_T and the local electron temperature. These dependences may be explicitly shown as (with the reasonable assumption that the local current density is fixed):

$$\chi = \chi_{an} L_o(1/L_T + 2/L_n)[1 - T_{crit}\nabla T_{crit}/(T\nabla T)]. \tag{7}$$

The parameters L_o and T_{crit} have been introduced to keep the equations dimensionally correct. They can be thought of approximately in the following way; For perturbative studies $L_o^{-1} =< 1/L_T + 2/L_n >_{equil}$ and $T_{crit} = T_{equil}$ and for incremental studies the parameters are approximately as defined above using the ohmic case in the scan.

For incremental transport studies (assuming profile resiliency) the strong correlation between T and ∇T means that the inverse dependence of the critical temperature gradient on T may be replaced by an inverse dependence on ∇T and the RLW model has the approximate form

$$\chi = \chi_{an}[1 - (\nabla T_{crit}/\nabla T)^2] \tag{8}$$

which may be compared to the incremental χ form

$$\chi = \chi^{inc}[1 - \nabla T_{crit}/\nabla T] \tag{9}$$

where the expression for χ^{inc} is exactly

$$\chi^{inc} = \chi_{an}(1 + \nabla T_{crit}/\nabla T). \tag{10}$$

Conversely, in perturbative heat pulse studies, the gradient term in the temperature scale length is important, but the T term in the critical gradient may be ignored. On TFTR the density pulse is weaker and much slower than the heat pulse (as on JET[18]), thus the perturbations to the term involving the density gradient may be ignored.

$$\chi^{HP} \approx \chi_{an}\left(1 + \frac{1 - \nabla T_{crit}/\nabla T}{1 + 2L_T/L_n}\right). \tag{11}$$

The RLW model, predicts that $\chi^{HP} \leq 2\chi^{inc}$ for $\nabla T \gg \nabla T_{crit}$ and $\chi^{HP} \approx \chi^{inc}/2$ for $\nabla T \approx \nabla T_{crit}$. In Fig. 1, the ratio of ∇T to ∇T_{crit} as predicted by the RLW model varies from unity (for the ohmic case) to about 5 for the highest beam power cases. This may appear surprising as ∇T changed by only a factor of two; however, the critical temperature gradient varies inversely with T, and hence ∇T_{crit} is a factor of two lower for the high power shots than for the ohmic shot. In contrast to the incremental χ model, for $\nabla T \gg \nabla T_{crit}$, as is the case for the higher power points in Fig. 1, this model predicts $\chi^{HP} \leq 2\chi^{PB}$

The two models investigated above were both inconsistent with the experimental data. Experimentally it was found that $\chi^{HP} \approx 5\chi^{PB}$, whereas the incremental-χ model predicted $\chi^{HP} = (1.5 - 2)\chi^{PB}$ and the RLW model predicts $\chi^{HP} \leq 2\chi^{PB}$. However, it was demonstrated that χ^{HP} and χ^{inc} are not in general the same for non-linear transport models. The simplest approach to interpreting the experimentally observed difference between χ^{HP} and χ^{inc} is to consider a generic power-law model of the form,

$$\chi \propto T_e^{\alpha} L_T^{-\beta}. \tag{12}$$

For this model $\chi^{HP} = (\beta + 1)\chi^{PB}$ and $\chi^{inc} = (\alpha + 1)\chi^{PB}$. Thus, the experimental data for the high temperature shot in Fig. 1 might be explained with $\alpha = 1$ and $\beta = 4$. This implies a very strong, perhaps unrealistic, non-linear dependence of the thermal diffusivity on the temperature gradient over a wide range in temperature gradients. Below, it will be shown that an even stronger non-linearity is required to duplicate the heat pulse shape, rather than just the time-to-peak, thus it seems very unlikely that simple non-linear transport models are responsible for the rapid heat pulse propagation observed on TFTR.

II. Experimental Heat Pulse Data

Heat pulse propagation studies on TFTR have been done in both ohmic and neutral beam heated plasmas. A large variation in the χ^{HP} has been observed; generally on TFTR the heat pulses propagate slower in the higher density or colder plasmas. While there is a tendency for χ^{HP} to increase and 'saturate' with higher beam power, there is still significant variation of χ^{HP} at beam powers up to $5 \times P_{OH}$.

In Fig. 2 is shown the χ^{HP} (determined from simple time-to-peak analysis) for the temperature scan data shown in Fig. 1. The incremental χ model predicts that the heat pulse propagation should be invariant over this range of heating power. Indeed, for powers above about 6 MW, the χ^{HP} is very similar for all shots. However, for the lower power (coldest) shots, the heat pulse propagation is somewhat slower. In Fig. 3a, the electron temperature profiles from before and $300\mu s$ after the sawtooth crash are shown for a high and low temperature beam heated plasma with a density of $< n_e >= 3.8 \times 10^{19}/m^3$. As can be seen the profile shapes, the inversion radii and the percent drop

in the central T_e are very similar for these shots. However, the heat pulses in the colder plasma propagated more slowly (Fig. 3b). These observations are not consistent with the incremental-χ model or other offset linear forms of non-linear transport models since even for the highest power shot shown here, ($P_{beam} = 19MW$) $\chi^{HP} > 5\chi_e^{PB}$ or $2.5\chi_e^{inc}$. They could, however, be qualitatively consistent with generalized non-linear models. This result will be discussed in more detail below.

The prediction of the RLW model regarding the scaling of χ^{HP} with density was checked by increasing the density at constant electron temperature. The gas feed was increased with increasing beam power so as to keep T_e roughly constant (Fig. 4a). The low density shot had $< n_e >= 4 \times 10^{19}/m^3$ which was increased to $< n_e >= 6 \times 10^{19}/m^3$. The higher density shot had a slower heat pulse propagation by roughly a factor of five (Fig. 4b) while the χ^{PB} remained nearly constant. The χ^{HP} was calculated by the extended-time-to-peak method[5] over the radial range 0.28m$< r <$ 0.47m. With this method $\chi^{HP} = L_{amp}V_{HP}$ where L_{amp} is the gradient scale length of the heat pulse peak amplitude and V_{HP} is the velocity of the heat pulse peaks. The RLW model predicts a weak dependence of χ^{HP} on density as $\nabla T_{crit} \propto n_e^{1/2}$. For this density scan the predicted changed in χ^{HP} is about 10% .

Heat pulse propagation is also found to vary in ohmic plasmas; however interpretation of the results is much more difficult. Separation of the heat flow in the electron and ion channels is not feasible and it is not possible to independently vary the electron density and temperature. The data from two shots at the extremes of an ohmic density scan are shown in figure 5a. For densities below about $< n_e >\approx 1.6 \times 10^{19}/m^2$ the heat pulses were ballistic (see next section). At the highest densities in this scan, $< n_e >\approx 3.1 \times 10^{19}/m^3$ the heat pulses were slower than at the lower densities, but still too fast to be consistent with χ^{PB} (Fig. 5b).

A. The Ballistic Response

In the preceding section it is clear that the heat pulse propagation is faster than might be explicable by the types of transport models described in Sec. I. That, however, is not the only problem with simple interpretations of the experimental heat pulses. A careful study of the shape of the heat pulses over the radial range $r_{mix} < r < 1.5r_{mix}$ shows[6] that the shape of the

heat pulses is not consistent with a simple diffusive process, *i.e.*, χ_e constant in time. The initial rate-of-rise of the heat pulse is much too fast, a feature described as the 'ballistic' effect.

On TFTR the sawteeth appear to be Kadomtsev-like[19,20] in that there is no observed direct deposition of heat beyond the mixing radius during the sawtooth crash (however on a timescale of hundreds of μsec after the sawtooth crash, heat is transported in a diffusive manner well beyond the sawtooth mixing radius). In Fig. 6 the electron temperature profiles before and after a typical sawtooth crash are shown. The sawtooth crash results in a sharp shoulder on the temperature profile at the mixing radius of about 0.29 m and in a hollow temperature profile in the core. This hollow profile is more consistent with reconnection-like models than with, for example, fully stochastic models of the sawtooth crash. However, measurements of the q profile find that $q(0) < 1$,[21,22] which casts serious doubts on reconnection models for the sawtooth crash. However, this observation makes the assumption that heat redeposition is confined to within r_{mix} at the sawtooth crash even less defensible.

Studies of heat pulse propagation on TFTR have been greatly improved over previous studies by the introduction of a GPC which can make fast, 4μsec measurements of the electron temperature profile. With this diagnostic it is possible to identify the location of the mixing radius, as well as make absolute measurements of the heat pulse amplitude *versus* minor radius. This diagnostic makes possible the quantitative measurement of the 'ballistic' component of sawtooth induced heat pulse propagation. This ballistic effect appears to be correlated with the strength of the m=1 precursor eigenmode beyond the mixing radius.[6,23]

In Fig. 7 the experimental heat pulses from the sawtooth in Fig. 6 are compared to simulated heat pulses using $\chi^{PB}(r)$. As well as propagating faster than the simulated heat pulses, the experimental heat pulses have a larger amplitude and a slower decay of amplitude with increased minor radius. In Fig. 8 is shown data taken at 100kHz during the sawtooth crash. Both the inboard and outboard electron temperature data from radii between r_{mix} and $1.4r_{mix}$ are shown. At the time of the crash (approximately 0.4 msec in the figure) a spike in the temperature lasting 20 - 30 μsec is observable on the outboard channels (0.31 and 0.37m); this temperature rise is not due to cross-field transport, but reflects the displacement of the flux surfaces

by the (m,n) = (1,1) precursor. Following the spike is a slower, axisymetric temperature rise over a period of 100 - 300 μsec. This is the ballistic response. The experimental data are compared to a simulation predicting what should have been observed had the heat pulses evolved with the power balance estimate for the electron thermal diffusivity, χ^{PB}. For example, at a minor radius of 0.42 m, the electron temperature increases by $\approx$ 170 eV in the 500μsec following the crash; in the simulation using χ^{PB} the change is less than 1 eV over the same interval, a factor of 200 too small. It will be shown below that this rate of temperature rise is also much larger than would be consistent with the χ^{HP} [$\equiv (r^2 - r^2_{mix})/9t_{peak}$] or χ^{inc} ($\equiv \partial Q_e/\partial(\nabla T)$) inferred for these plasmas.

Parameter Dependence of the Ballistic Effect

Determination of the strength of the ballistic effect is difficult as even the most strongly ballistic cases appear, at least superficially, to be 'diffusive' when viewed with relatively slow (<5 kHz) diagnostics. Only by careful comparison of the experimental data to heat pulses simulated with various linear and nonlinear models is it possible to show clearly that the heat pulses have a ballistic component which cannot be modeled with a pure diffusion code. Likewise, the lack of fast temperature profile information introduces uncertainty in determining the location of the mixing radius, e.g., looking at the rate-of-rise of the heat pulse with a relatively slow, 5kHz, diagnostic[24,25] to determine the mixing radius will result in an incorrect answer. Any uncertainty in the location of the 'mixing radius' introduces further difficulties in quantifying the strength of the ballistic effect.

The origin of the ballistic response is not known at this time, however recent works by several authors[6,23,26,27] have suggested a connection between the strength of the $m = 1$ eigenmode beyond the $q = 1$ surface and the amount of stochastic enhancement of the heat pulse propagation. With fast (>100kHz) measurements of the electron temperature profile evolution in plasmas rotating fast relative to the sawtooth crash times it is possible to directly measure the poloidal structure of the n=1 sawtooth precursor.[20] By examination of the radial displacement of contours of constant electron temperature, it is possible to infer the displacement in the flux surface, $\xi(r)$, resulting from the $m = 1$ precursor to the sawtooth crash. In Fig. 9 the

temperature profiles before and $\approx 300\mu$sec after a sawtooth crash are shown. In Fig. 10 the inferred displacement of the flux surfaces on the low field side due to the mode is shown. As opposed to the 'tophat' eigenmode structure expected in cylindrical low β models, this precursor extends well beyond the $q = 1$ surface to nearly $r = 0.4m$. A simulation using the experimental heat pulse at the minor radius $r = 0.28m$ as the inner boundary condition is shown in Fig. 11a. The multiplier of 15 on χ^{PB} is chosen to match the time-to-peak at $0.56m$. The rate of rise and amplitude of the simulated heat pulses is much smaller than experimentally observed for the channels further out. The situation is similar if the experimental heat pulse at $r = 0.35m$ is used as a boundary condition. However, using the data from $r = 0.42m$, as shown in Fig. 11b, it is possible to find good agreement, in this case using an effective $\chi_e = 10\chi^{PB}$. Thus, beyond the radial region most strongly affected by the precursor activity, the heat pulse could be considered roughly diffusive.

This result is suggestive that magnetic activity induced by the sawtooth crash does play a role in the subsequent heat pulse propagation. However, extension of the eigenmode beyond the $q = 1$ surface does not guarantee that there will be stochasticity in that region. Further, such measurements of $\xi(r)$ are difficult to make, typically only being possible in beam heated plasmas which rotate relatively fast.

III. Heat Pulse Simulations

In this section numerical simulations based on models for the heat transport will be compared to the experimental data in order to gain deeper insight into the nature of the heat pulse propagation. The variety of models purporting to describe thermal transport in tokamaks is large; by necessity we will restrict this study to several representative models which we judge to be most relevant. We will first investigate the possibility that the thermal diffusivity is transiently affected by the passage of the heat pulse, most probably through the increase in the electron temperature gradient (∇T_e). The dependence of χ_e on the temperature gradient can be arbitrarily complex, and we will only try two specific models, the incremental-χ model and a generic power law model. We will show that the experimental sawtooth induced heat pulse propagation is inconsistent with the χ^{inc} determined from the power scan studies. We will further show that the shape of the heat pulses cannot

be reproduced with any reasonable model which relies only upon an implicit ∇T_e dependence in χ_e. We will then look for an explicit time-dependent form for χ_e, beginning with an analytic expression suggested in an earlier paper by Fredrickson, *et al.*[6] which gave *qualitative* agreement with the ballistic effect at $r \approx 1.4 r_{mix}$ and the subsequent heat pulse propagation out to $r \approx 2.0 r_{mix}$. By adjusting the parameters in the expression it is possible to find a *quantitatively* correct simulation of both the ballistic response between $r = r_{mix}$ and $r \approx 1.4 r_{mix}$ as well as the heat pulse in the outer region. While a good fit to the experimental heat pulses may be found in this way, this approach does not address the physical mechanism responsible for the enhancement directly, as has been discussed previously.[6] The first two models apply in general to transient perturbations of the temperature profile, the last model, of course, is only relevant to studies of sawtooth induced heat pulse propagation.

The object of these simulations is to develop a self-consistent model for the thermal transport which can both describe the equilibrium plasma as well as the evolution of the sawtooth induced perturbations. The numerical simulation code solves the 1-fluid (electron) heat transport equation (Eq. 1). Approximate fits to the experimental density profile, heating profile Q and equilibrium χ profile are found using analytic expressions. The sawteeth are simulated as an energy conserving instantaneous reconnection. The mixing radius as well as the hollowness of the post sawtooth profile are chosen to best match the experimental data. The sawtooth crash in the simulation does not transport heat beyond the mixing radius. The radial grid in the code has a 1 cm spatial resolution and a Dirichlet ($\partial T/\partial t = 0$) boundary condition is enforced at $r = 1$ m. The typical TFTR plasma has a minor radius of 0.8 m; thus the code allows finite temperature and heat pulse amplitude at the plasma 'edge'.[4] This approach results in smaller reflections from the plasma boundary in these simulations than would the condition that $\tilde{T}/T = 0$ at the edge of the plasma. However, the actual boundary condition has not been measured experimentally for these shots (due primarily to a low signal-to-noise at the plasma edge for ECE temperature measurements). The modifications to the above formula necessary to simulate the various models will be discussed below.

An important input to the simulation code is the proper reconnection or mixing radius, r_{mix}. The use of a mixing radius larger than the experimental

one will increase the heat pulse amplitude and shorten the time-to-peak, thus at larger minor radius the effect will be similar to that due to the ballistic response. Experimentally determination of the location of the mixing radius is simple with fast temperature profile data. The temperature profile is flat or slightly hollow within the mixing radius following the sawtooth crash and the mixing radius is defined as the radius at which the sharp 'shoulder' appears on the temperature profile (c.f. Fig. 6). This definition of the mixing layer is basically similar to that introduced by Sips and Lopes Cardozo where the mixing radius is defined as 'the radius out to which there is an immediate response of T_e to the crash'.[24] However, as can be seen from the data shown in Fig. 8, a digitizing rate of at least 100kHz, not the 5kHz typically used by Sips *et al.*, is necessary to properly measure the mixing radius.

The sawtooth repetition time in the experiment was about 250msec; however the reheat had saturated at about 100msec, so to reduce computation time, a sawtooth period of 100msec was used in the simulations. A few simulations were done with a 200msec sawtooth period, and as expected there was no effect on the heat pulse propagation. Experimentally, the reconnection was observed to leave the temperature profile temporarily hollow within the mixing radius, and a parameter to simulate this hollowness was included in the simulation code.

In addition to the above simulations, various 'perturbative' simulations using the linearized transport equations are useful. For the investigation of the incremental-χ model both an initial value, perturbative simulation and a driven boundary condition perturbative simulation (using experimental data) were performed. These simulations will be discussed in more detail below.

A. Non-linear χ Models

The non-linear χ_e models are motivated in part by the observation that an implicit ∇T dependence in χ_e would result in a difference in the effective thermal transport coefficients for equilibrium *versus* transient heat flows. This is consistent with, but not proven by, the approximate offset linear scaling of the (one fluid) heat flux with $n\nabla T$ reported on JET and is also suggested by the many observations of profile consistency.[7-10] However, as was demonstrated above, it is very difficult to distinguish between the various possible non-linear scalings of the *electron* heat flux based upon power scan

analyses and the relationship between χ^{HP} and χ^{inc} depends on the transport model assumed.

There is both experimental and theoretical support for the suggestion that $\chi = f(\nabla T)$ (c.f. Fig. 1). There are theoretical models which predict a temperature gradient dependence in the electron thermal transport, *e.g.*, η_e models[28] and semi-empirical models such as the RLW model.[17] In the η_e models, that dependence is weak, predicting roughly a dependence of χ_e on the temperature gradient to the power of 1-1.5. Experimental studies of the equilibrium dependence of χ_e on electron temperature suggest a weak scaling, with $\chi_e \propto T_e^{0-1}$ (*e.g.*, Fig. 1). In equilibrium, the temperature and temperature gradient are very strongly correlated, and it is not possible to separate a temperature gradient dependence from a temperature dependence. The Rebut-Lallia-Watkins model is closest to a pure incremental-χ model, where the diffusivity has an offset-linear dependence on ∇T of the form

$$\chi_e(r,t) = \chi^{inc}\left(1 - R\frac{\nabla T_o}{\nabla T}\right), \qquad \nabla T > \nabla T_o \tag{13}$$

where $R \equiv \nabla T_{crit}/\nabla T_o$ and T_o is the equilibrium temperature. The ratio R and ∇T_{crit} are adjustable parameters used to fit the experimentally measured χ^{HP} and χ_e^{PB}, respectively. This functional form for $\chi_e(\nabla T)$ has the useful mathematical property that the diffusion equation, outside the mixing radius, is exactly separable into a part describing the equilibrium heat transport with an effective $\chi_e^{PB} = \chi^{inc}(1 - R)$ and a 'transient' part with $\chi_e^{HP} = \chi^{inc}$. As mentioned previously, a constraint on this model is that these equations are only valid beyond the mixing radius where the expression for χ_e is positive. In any region of the plasma where the temperature gradient falls below $R\nabla T_o$ this model predicts a negative value for χ_e.

Sips *et al.* have attempted to simulate the heat pulse data shown in Fig. 7 using an incremental-χ model of the form $\chi^{inc} = 1.0 + 14\sqrt{r/a}$. In their initial value simulations they found it necessary to use a mixing radius of $r_{mix} = 0.34m$.[24] From the fast temperature profile data, however, the mixing radius can be determined quite accurately as $r_{mix} = 0.29 \pm 0.01$m (Fig. 12). With the proper mixing radius and this model for χ^{inc} the amplitude of the heat pulse is too small and the rate-of-rise is too slow at the minor radius of about $0.4m$. Thus, by using a mixing radius 20% larger, $r_{mix} = 0.34m$, than the true mixing radius, $r_{mix} = 0.29m$, Sips and Lopes

Cardozo were able to approximately simulate the effects of the ballistic response for $r > 1.4r_{mix}$,[24,25] *i.e.*, outside the region of the strong ballistic response. If the ballistic effect is properly simulated within $1.4r_{mix}$, it is possible to approximately simulate the heat pulses in the region beyond $r \approx 1.4r_{mix}$ with a number of diffusive and non-diffusive models.

The simulation described above by Sips and Lopes Cardozo was a linearized initial value simulation or perturbative simulation. For a non-linear simulation of heat pulse propagation with this model, it is necessary to deal gracefully with the constraint that $\chi_e > 0$. In previous perturbative simulations, the approach has been to use a very low value of χ_e within the mixing radius. In the same spirit, the non-linear simulations were done with the model

$$\chi(r,t) = 0.001 + \chi^{PB}(r)(\nabla T/\nabla T_o)^4 \qquad \nabla T < \nabla T_o. \tag{14}$$

The actual $\chi_e(\nabla T)$ used is shown in Fig. 13. In the same figure, for comparison, is the χ_e *vs.* ∇T for the other two models discussed below.

Simulations using the χ^{inc} determined from the temperature scans at constant density discussed above show that the heat pulses propagate approximately a factor of two slower than the experimental data. To match the time-to-peak of the experimental data, it is necessary to use $\chi_e^{HP} = 2.5\chi^{inc} = 5\chi_e^{PB}$, i.e., $R = 0.8$. In Fig. 14 the heat pulses simulated with this model are compared to the experimental heat pulses. While the time-to-peak and general shape of the heat pulses agree fairly well, the heat pulses are about a factor of two too small. The conclusion is that while this model does enhance χ, creating a 'ballistic' effect, the enhancement in χ is too weak near the mixing radius and occurs too late at larger radii. At the minor radius of 0.42m, the increase is only 30 eV in the 500 μsec after the crash compared to the experimentally measured increase of 170 eV.

In the context of the simulations as done so far, there are no adjustable parameters available to improve the fit with this simulation. However, by using a stronger non-linear power-law model

$$\chi_e(r,t) = \chi_e^{PB}(\nabla T/\nabla T_o)^4 \tag{15}$$

it is possible to increase the enhancement in χ near the mixing radius. (Here ∇T_o is the equilibrium temperature gradient.) In Fig. 15 the heat pulses simulated with this model are compared to the experimental heat pulses. At larger radii, the agreement is of similar quality to the χ^{inc} simulation of

figure 14. However, near the mixing radius, this power law model gives a somewhat stronger 'ballistic' effect. The exponent of 4 was chosen such that if this model were linearized to the incremental-χ form, the result would be equivalent to Eq. (9). In general, linearization of power-law models of the form $\chi \propto \nabla T^{\alpha}$ to the incremental χ_e form gives:

$$R = \alpha/(\alpha + 1) \tag{16}$$

and

$$\chi^{inc} = (1 + \alpha)\chi_e^{PB}. \tag{17}$$

Thus, for $R = 0.8$, as used in the χ^{inc} simulation, $\alpha = 4$.

The cause of the difference between the incremental and power law models is clear; while the linearization of this model is identically the χ^{inc} model, the linearization breaks down near the mixing radius where the change in temperature gradient can be more than a factor of two. Thus the amount of enhancement to χ_e is much greater with this model than with the χ^{inc} model near the mixing radius and the heat pulses come closer to matching the ballistic response. However, even with a dependence on ∇T to the fourth power this model still does not give a strong enough 'ballistic' effect. Obviously a much stronger enhancement in χ_e, i.e., a stronger non-linearity than $(\nabla T)^4$ is required to match the experimentally measured heat pulse amplitude and ballistic contribution.

Rather than investigate more complicated dependencies of χ_e on ∇T, we will use simulations using the linearized equations to determine to what extent the heat pulses are actually purely diffusive, i.e., describable by a diffusion equation (linearized) with a time-independent χ_e. We will begin with driven boundary condition simulations. We use the experimentally measured heat pulse at a given radius as the inner boundary condition in the simulation. As before, we will use $\chi^{eff} = 5\chi^{PB}$, or $\chi^{eff} = 2.5\chi^{inc}$, to match the time-to-peak.

In Fig. 16a the heat pulses are simulated using the experimental heat pulse immediately outside the mixing radius, at $r = 0.31m$. In χ_{inc} models the heat pulse propagation should be diffusive beyond that point. While the heat pulse amplitude and time-to-peak agree fairly well, there is still a significant discrepancy in the rate of rise of the heat pulse at $r = 0.36m$ (shown as the shaded region in Fig. 16a). The obvious conclusion is that the heat pulse propagation is not diffusive between $0.31m$ and $0.36m$. The

simulations can be done using the experimental heat pulses at larger minor radii. In this manner it is found that only beyond $r = 0.42m$ are the heat pulses 'diffusive' (Fig. 16b) and the χ_e^{HP} for this model is $\approx 5\chi_e^{PB}$ or $\approx 2\chi^{inc}$. (For the RLW model $\chi^{HP} \leq 2\chi^{PB}$ with $\nabla T = 5\nabla T_{crit}$.)

B. Analytic Approximation to $\chi(r,t)$

In the previous section various models with implicit transient enhancements in χ resulting from assumed non-linearities in the thermal diffusivity were investigated. The principal failure of these models was that the enhancement in χ near the mixing radius was too weak, resulting in a heat pulse amplitude which was too small. While very strong non-linearities in the heat flux might explain this ballistic effect, in the case of sawtooth induced heat pulse propagation, it is of course possible that the sawtooth crash transiently enhances the diffusivity beyond the mixing radius following the sawtooth crash. In the reconnection model of the sawtooth crash an enhancement in the thermal diffusivity is predicted in numerical studies. The enhancement is due to the effect of finite pressure and toroidicity[23,26,27] on the $m = 1$ sawtooth precursor, leading to a stochastic magnetic field structure. The theoretical model is sufficiently complex that no quantitative predictions of the level of stochasticity, nor of the effect of said stochasticity on thermal transport can be made. Qualitatively, it might be expected that the stochastic regions would most strongly affect *electron* thermal transport and have much less of an effect on ion thermal transport or particle transport. Ion heat pulse propagation measurements have not been made, but the particle pulse does move an order of magnitude slower than the electron heat pulse in TFTR (and JET[18]). Likewise, the stochastic regions would be expected to be strongest near the mixing radius, which will be seen to be consistent with the experimental observations. Here we will use an explicit model for the temporal and spatial enhancement in χ_e and attempt to reproduce the heat pulse shape just outside the mixing radius. We will also demonstrate that at larger minor radii ($r > 1.4r_{mix}$) the shape of the heat pulse is relatively insensitive to the form of the enhancement.

A very simple analytic expression for a time dependent χ_e with only three adjustable parameters has been found to give a very good qualitative fit to

the experimental data. The time dependant χ_e has the form

$$\chi_e(r,t) = \chi_e^{PB}(r)[1 + \delta exp(-t/\tau - \kappa r^2)]. \tag{18}$$

This form of the $\chi(r,t)$ gives an enhancement in χ_e that is strong near the mixing radius, and falls off rapidly with larger r. Near the mixing radius, the enhancement is necessary for only a short time ($\approx$ 1 msec) following the sawtooth crash. With this model, the simulated heat pulses were found to have a rapid temperature rise, even at large minor radius and a relatively slow fall-off in amplitude with minor radius. The equilibrium temperature profile is accurately simulated as well as the sawtooth heat pulse. While this expression enhances $\chi(r,t)$ in the core, it is found that the simulations are insensitive to the enhancement in this region. The enhancement can be turned off for $r < 0.8r_{mix}$ with no measurable effect on the heat pulse shapes beyond r_{mix}. This is to be expected as the temperature gradient is very small in the core region.

In Fig. 17 the simulated and experimental temperature perturbations are compared and in Fig. 18 the temporal evolution of the perturbations are compared on a shorter timescale. On both short and long timescales, the quantitative agreement is very good. This form of the χ enhancement was chosen to best reproduce the ballistic effect, *i.e.*, to give the best simulation of the heat pulse at $r = 0.36m$. The qualitative difference between this model and the implicit models tested above are that the perturbation to χ_e occurs simultaneously at all radii, and that the enhancement is much stronger near the mixing radius with this model.

As is seen in Fig. 17, this model simulates the heat pulses quite well at larger minor radius. In particular, it has been shown above that the heat pulses beyond about $r = 0.42m$ pulses can be fit with an incremental-χ model. As can be seen in Fig. 17 the simulated heat pulses with this explicit model agree very well with the experimental data out to $r = 0.52m$, thus, the shape of the heat pulses in this region is not particularly sensitive to the exact form of the enhancement in χ. This result is contrary to what has previously been assumed[25] and calls into question the usefulness of studying the heat pulses in this region. That is, it may be possible to demonstrate that the heat pulses are *consistent* with a particular model, however, it is not possible to prove that only one model could explain the data.

IV. Summary

Simple non-linear models, such as the incremental-χ model or the Rebut-Lallia-Watkins model fail to reproduce the time behavior of the heat pulses and predict too small an amplitude of the heat pulse near the mixing radius. The heat pulses at radii greater than about $1.4r_{mix}$ can be simulated with non-linear models. However, models with unacceptably strong non-linearities are required; in the outer region, $r > 1.4r_{mix}$, models with a dependence on the temperature gradient to the fifth (and higher) power are required.

There is strong circumstantial evidence to support sawtooth induced enhancements in electron thermal transport in the ballistic region, *i.e.*, typically between r_{mix} and $1.4r_{mix}$ in beam heated TFTR plasmas. There is, at present, no way to verify such a hypothesis, nor to prescribe boundaries beyond which such an effect may no longer be important. Further, because very different time-dependent forms of χ can result in qualitatively similar heat pulse shapes, there is no justification for claiming that beyond, for example, $r = 1.4r_{mix}$ the transport is diffusive.

More generally, it has been shown that the application of knowledge acquired from transient transport studies to equilibrium confinement scaling is not direct. Transient studies break constraints on plasma parameters that are present in equilibrium studies. Thus, the χ^{inc} determined from equilibrium temperature scans and the χ^{HP} determined from transient transport studies are only indirectly related. Other effects which have recently been invoked in the study of heat pulse propagation[12,29,30] may still be important in understanding transient transport phenomena, but great care must be exercised in their application to the analysis of sawtooth-induced heat pulse propagation.

While these observations pertain to the TFTR plasmas discussed above, the possibility that sawteeth can directly affect the heat pulse propagation should be of concern in any study of sawtooth induced heat pulse propagation and possibly in any heat pulse study where sawteeth are present. While modulated electron cyclotron heating experiments present an attractive alternative to sawtooth induced temperature perturbations, the effects of possible sawtooth induced enhancements in the thermal transport on the effective ECH deposition must be considered.

Acknowledgments

The authors would like to thank W. Stodiek, and J. Callen for many useful discussions and suggestions. This work was supported by US DOE Contract No. DE-AC02-76CH0-3073.

References

[1]Liewer, P. C., Nucl. Fusion **25** (1985) 543.

[2]Callen, J. D. and Jahns, G. L., Phys. Rev. Lett. **38** (1977) 971.

[3]Jahns, G., Soler, M., et al., Nucl. Fusion **18** (1978) 609.

[4]Fredrickson, E. D., Callen, J. D., McGuire, K.M., Bell, J. D., Colchin, R. J., Efthimion, P. C., Hill, K. W., Izzo, R., Mikkelsen, D. R., Monticello, D. A., Paré, V., Taylor, G. and Zarnstorff, M., Nucl. Fusion **26** (1986) 849.

[5]Tubbing, B. J. D., Lopes Cardozo, N. J. and Van Der Wiel, M. J., Nucl. Fusion **27** (1987) 1843.

[6]Fredrickson, E. D., McGuire, K. M., Cavallo, A., Budny, R., Janos, A., Monticello, D., Nagayama, Y., Park, W., Taylor, G., and Zarnstorff, M. C., Phys. Rev. Lett. **65** (1990) 2869.

[7]Fredrickson, E. D., McGuire, K. M., Goldston, R. J., et al., Nucl. Fusion **27** (1987) 1897.

[8]Taylor, G., Fredrickson, E. D., Grek, B., Goldston, R. J., et al., Nucl. Fusion **29** (1989) 3.

[9]Becker, G., Nucl. Fusion **31** (1991) 663.

[10]Düchs, D. F., Stringer, T.E., Taroni, A., Bursati, M., Gottardi, N., Hellsten, T., Tibone, F., at 11th Int. Conf. on Plasma Phys. and Cont. Nucl. Fusion Research, Kyoto, Japan, 13-20 Novermber 1986 Vol. I, 325.

[11]Lopes Cardozo, N. J., Sips, A. C. C., Costley, A. E., Hogeweij, G. M. D., and O'Rourke, J., in *Proceeaings of the European Physical Society*, Berlin, Vol. I, (1991) 193.

[12]Gentle, K. W., Phys. Fluids **31** (1988) 1105.

[13]Goedheer, W. J., Nucl. Fusion **26** (1986) 1043.

[14]Bell, J.D., Dunlap, J. L., Pare', V. K., et al. Nucl. Fusion **24** (1984) 997.

[15]Riedel, K.S., Eberhagen, A., Gruber, O., Lackner, K., *et al.*, Nucl. Fusion **28** (1988) 1509.

[16]Efthimion, P. c., Mansfield, D. K., Stratton, B. C., Synakowski, E., *el al.*, Phys. Rev. Lett. **66** (1991) 421.

[17]Rebut, P. H., Watkins, M. L., Gambier, D. J., and Boucher, D., Phys. Fluids B **3** (1991) 2209.

[18]Lopes Cardozo, N. J. and de Haas, J.C.M., Nucl. Fusion **30** (1990) 521.

[19]Kadomtsev, B. B., Fiz. Plazmi Vol. 1 (1975) 710; Sov. J. Plasma Phys. 1(1975) 389.

[20]Nagayama, Y., McGuire, K.M., Bitter, M., Cavallo, A. et al., Phys. Rev. Lett. **67** (1991) 3527.

[21]Soltwisch, H. and Stodiek, W., in Plasma Physics and Controlled Nuclear Fusion Research 1986 (*Proc. 11th Int. Conf. Kyoto, 1986*) (1987) Vol. I 263.

[22]Batha, S., Levinton, F., Bell, M., Kessel, C., and Weiland, R. M., in *Bull. Am. Phys. Soc.* **37** (1992) 1481.

[23]Park, W., Monticello, D. A., Fredrickson, E. D., and McGuire, K. M., Phys. Fluids B **3** (1991) 507.

[24]Sips, A. C. C., Lopes Cardozo, N. J., Costley, A. E., Hogeweij, G. M. D., and O'Rourke, J., in *Proceedings of the European Physical Society*, Berlin, Vol. I, (1991) 193.

[25]Lopes Cardozo, N. and A. C. C. Sipps, Plasma Physics and Controlled Fusion **33** (1991) 1337.

[26]Aydemir, A. Y., Wiley, J.C., and Ross, D. W., Phys. Fluids B **4** (1989) 774.

[27]Baty, Proceedings of the 17th European Physical Society Conf. on Controlled Fusion and Plasma Heating, Amsterdam, Vol. 14B, Part II (1990) 889.

[28]Guzdar, P. N., Liu, C. S., Dong, J. Q., and Lee, Y. C., Phys. Rev. Lett. **57** (1986) 2819.

[29]Hossain, M., Kress, M., Hu, P. N., Blank, A. A., and Grad, H., Phys. Rev. Lett. **58** (1987) 487.

[30]Bishop, C. M. and Conner, J. W., Plasma Physics and Controlled Fusion, **32** (1990) 203.

List of Figures

Figure 1 Q *vs.* $n\nabla T$ at three radii for an electron temperature scan at constant density. The ohmic points in the scan are represented by open symbols and the points with NBI by closed circles. The temperature scan data can be equally well fit by the χ^{inc} model or a linear dependence of χ on T.

Figure 2 The χ^{HP} determined from time-to-peak analysis vs. the ratio of the temperature gradient to the critical temperature gradient.

Figure 3a The electron temperature profiles from before (solid line) and $\approx$ 300μs after (dashed line) sawtooth crashes in beam heated plasma at similar density (58554,58564). Parameters for this shot were $< n_e >= 3.8 \times 10^{19}/m^3, I_p = 1.8MA, P_{NBI} = 4MW$ and $17MW$.

Figure 3b Comparison of the heat pulses for the sawteeth shown in Fig. 3a. The dashed curve is for the low temperature case.

Figure 4a The electron temperature profiles from before and 300μs after a sawtooth crash in 1.8 MA beam heated plasmas (62270,62248). The density and beam power for these shots were, respectively, $< n_e >= 4 \times 10^{19}/m^3$ and $6 \times 10^{19}/m^3, P_{NBI} = 7.5MW$ and $15MW$.

Figure 4b Comparison of the heat pulses for the sawteeth shown in Fig. 4a. The dashed curve is for the low density case.

Figure 5a Temperature profiles before and after the sawtooth crash for a high and low density ohmic plasma (45455,45450). The lower density case has the higher temperature.

Figure 5b Comparison of the heat pulses for the high density (solid line) and low density (dashed line) sawteeth shown in Fig. 5a.

Figure 6 Profiles of the electron temperature before (solid) and 200μsec after (broken) a sawtooth crash (The parameters for this shot were I_p = 1.7 MA, $q(a)$ = 4.4, NBI power = 19 MW, a = 0.8 m, R = 2.45 m and B_T = 4.7 Tesla.)

Figure 7 Comparison of heat pulse data from ECE emission (solid line) to simulated heat pulses (dashed line) where the power balance thermal diffusivity profile has been used, $\chi(r) = (0.3 + 9(r/a)^2)e^{(2.6(r/a)^2)}$.

Figure 8 The heat pulses shown in Fig. 7, but now with faster sampling showing the ballistic response (solid line) and the simulated heat pulse (dashed line).

Figure 9 The electron temperature profiles from before and $\approx 300\mu s$ after a sawtooth crash in a beam heated plasma. Parameters for this shot were $< n_e >= 4.0 \times 10^{19}/m^3$, $I_p = 1.7MA, P_{NBI} \approx 28MW$.

Figure 10 The radial displacement of the constant temperature surfaces, $\xi(r)$ on the outboard (low field) side due to the (m,n)=(1,1) sawtooth precursor.

Figure 11a Comparison of the experimental heat pulses (solid line) to simulated heat pulses (dashed line) using the experimental pulse shape at $r = 0.28m$ as the inner boundary condition.

Figure 11b Comparison of the experimental heat pulses (solid line) to simulated heat pulses (dashed line) using the experimental pulse shape at $r = 0.42m$ as the inner boundary condition.

Figure 12 Comparison of the radial profiles of the electron temperature from experiment and the simulations shown in Figs. 7,8,11 and 14 through 18 before and after the sawtooth crash as well as the profile after the crash as used by Sips and Cardozo.[24]

Figure 13 The normalized χ vs. the normalized ∇T for the power law model and the χ^{inc} model. Also shown is normalized χ vs. the normalized ∇T at a radius of $0.34m$ for the simulation shown in Fig. 17.

Figure 14 Comparison of the experimental heat pulses (solid line) with a non-linear simulation (dashed line) using $\chi(r,t) = 5\chi^{PB}(1 - .8\nabla T_o/\nabla T)$ for $\nabla T > \nabla T_o$.

Figure 15 Comparison of the experimental heat pulses (solid line) with a non-linear simulation (dashed line) using $\chi(r,t) = \chi^{PB}(r)(\nabla T/\nabla T_o)^4$ for $\nabla T > 0$.

Figure 16a Comparison of experimental (solid line) and simulated (dashed line) heat pulses where the boundary condition at $r = 0.31m$ is the experimental shape of the heat pulse and $\chi = 5\chi^{PB}$.

Figure 16b Comparison of experimental (solid line) and simulated (dashed line) heat pulses where the boundary condition at $r = 0.42m$ is the experimental shape of the heat pulse and $\chi = 5\chi^{PB}$.

Figure 17 Comparison of the experimental heat pulses from Fig. 6-8 (solid line) with heat pulses simulated using a time dependent thermal diffusivity of the form $\chi(r,t) = \chi^{PB}(r)(1 + 35exp(-1000t - 16r^2)$ (dashed line).

Figure 18 Comparison of the experimental (solid line) and simulated

(dashed line) fast time behaviour of the heat pulses for radii less than $1.4r_{mix}$.

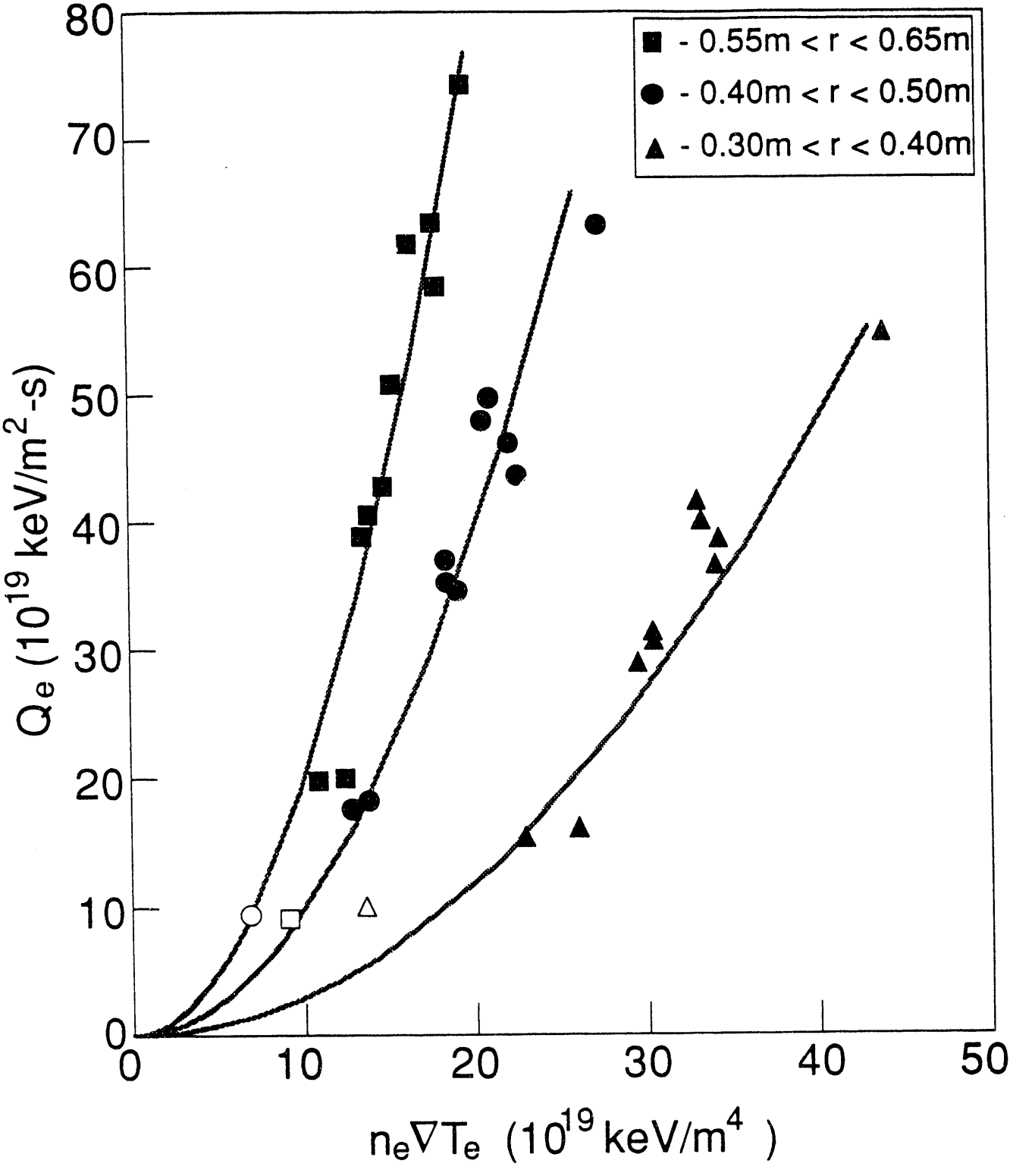
■ - 0.55m < r < 0.65m
● - 0.40m < r < 0.50m
▲ - 0.30m < r < 0.40m
Q_e (10^{19} keV/m^2-s)
$n_e \nabla T_e$ (10^{19} keV/m^4)
0
10
20
30
40
50
60
70
80

Figure 1

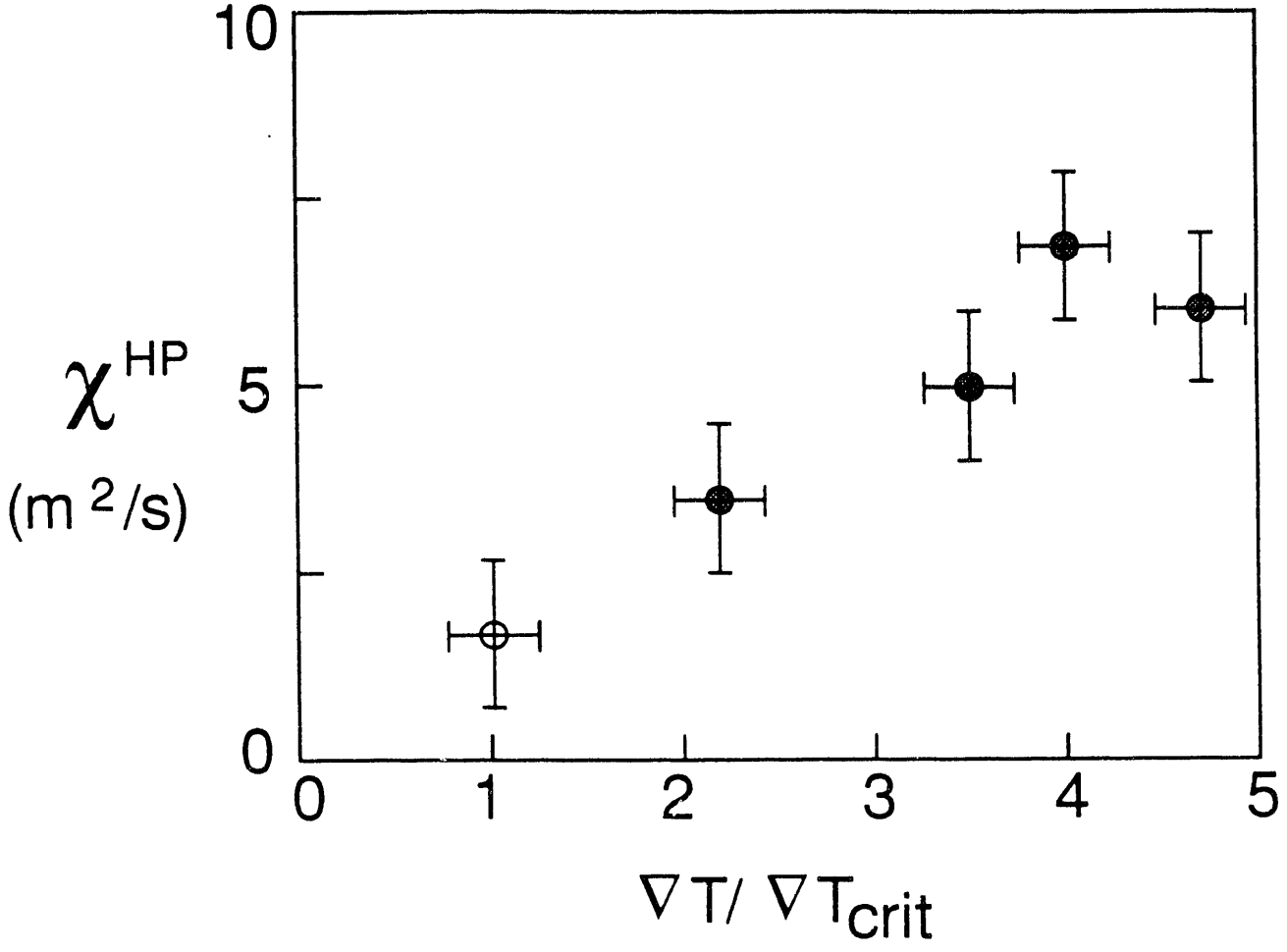

Figure 2

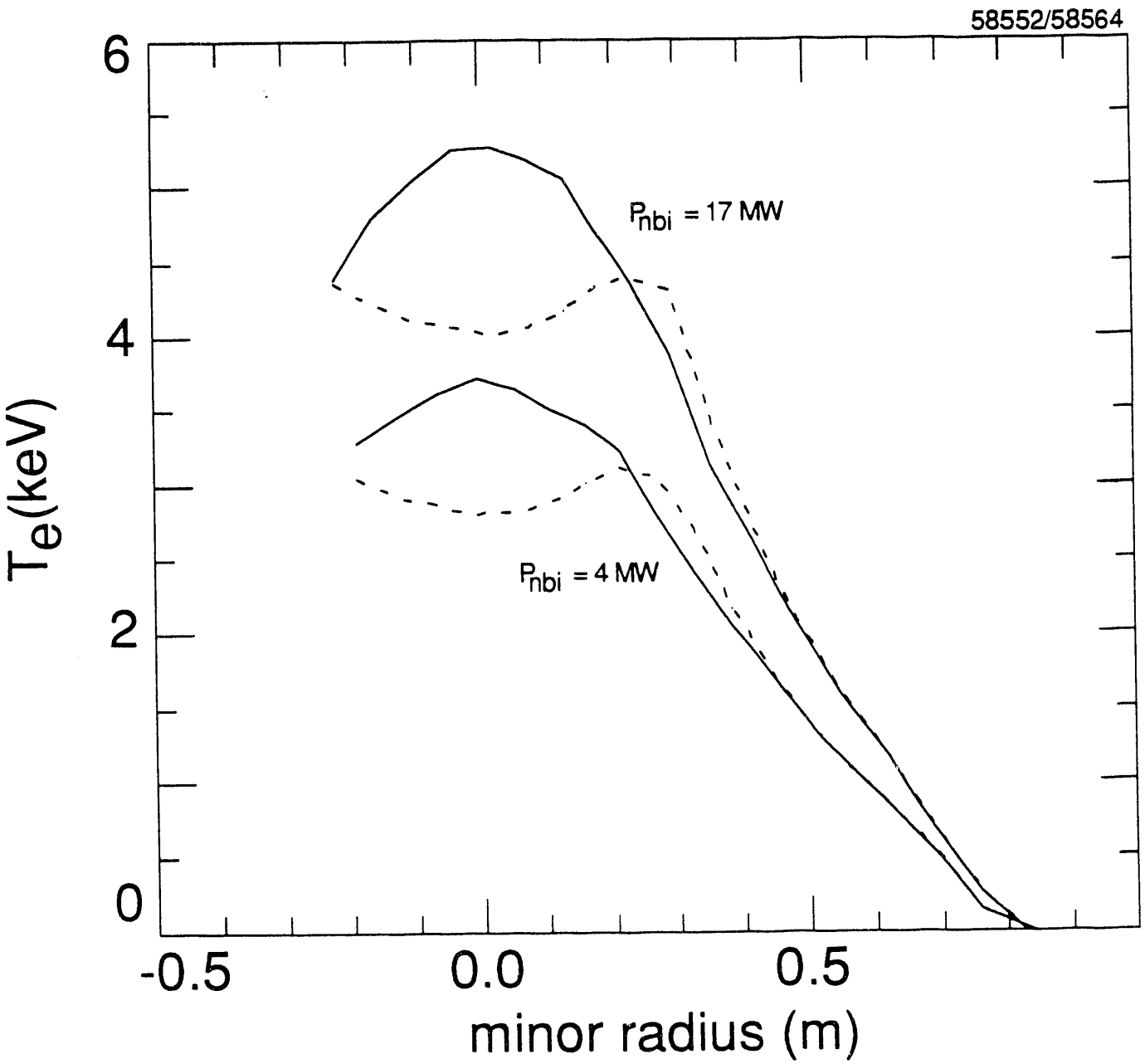

Figure 3a

1.007/1.013

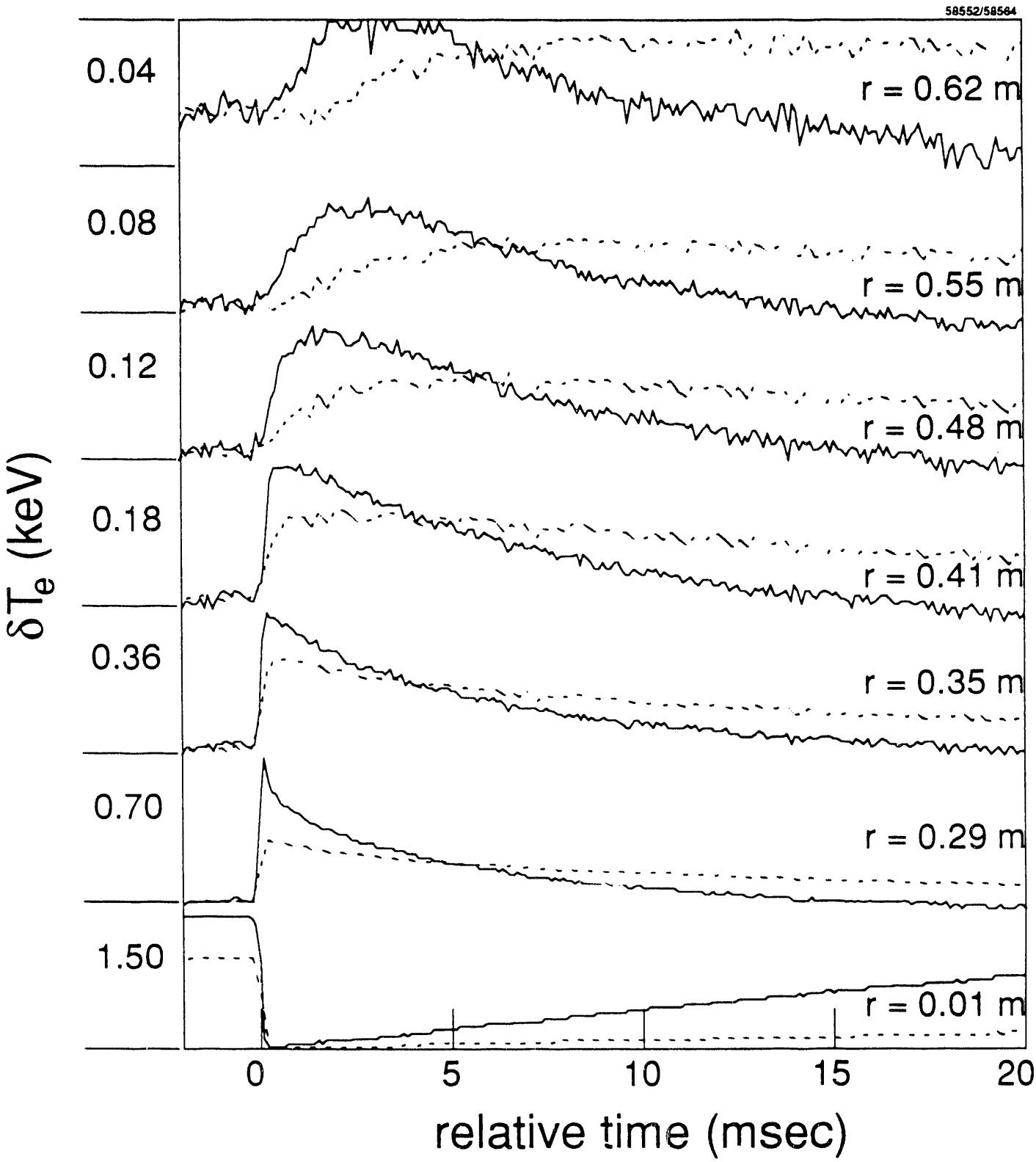
58552/58564
0.04
0.08
0.12
0.18
0.36
0.70
1.50
r = 0.62 m
r = 0.55 m
r = 0.48 m
r = 0.41 m
r = 0.35 m
r = 0.29 m
r = 0.01 m
δTe (keV)
0
5
10
15
20
relative time (msec)

Figure 3b

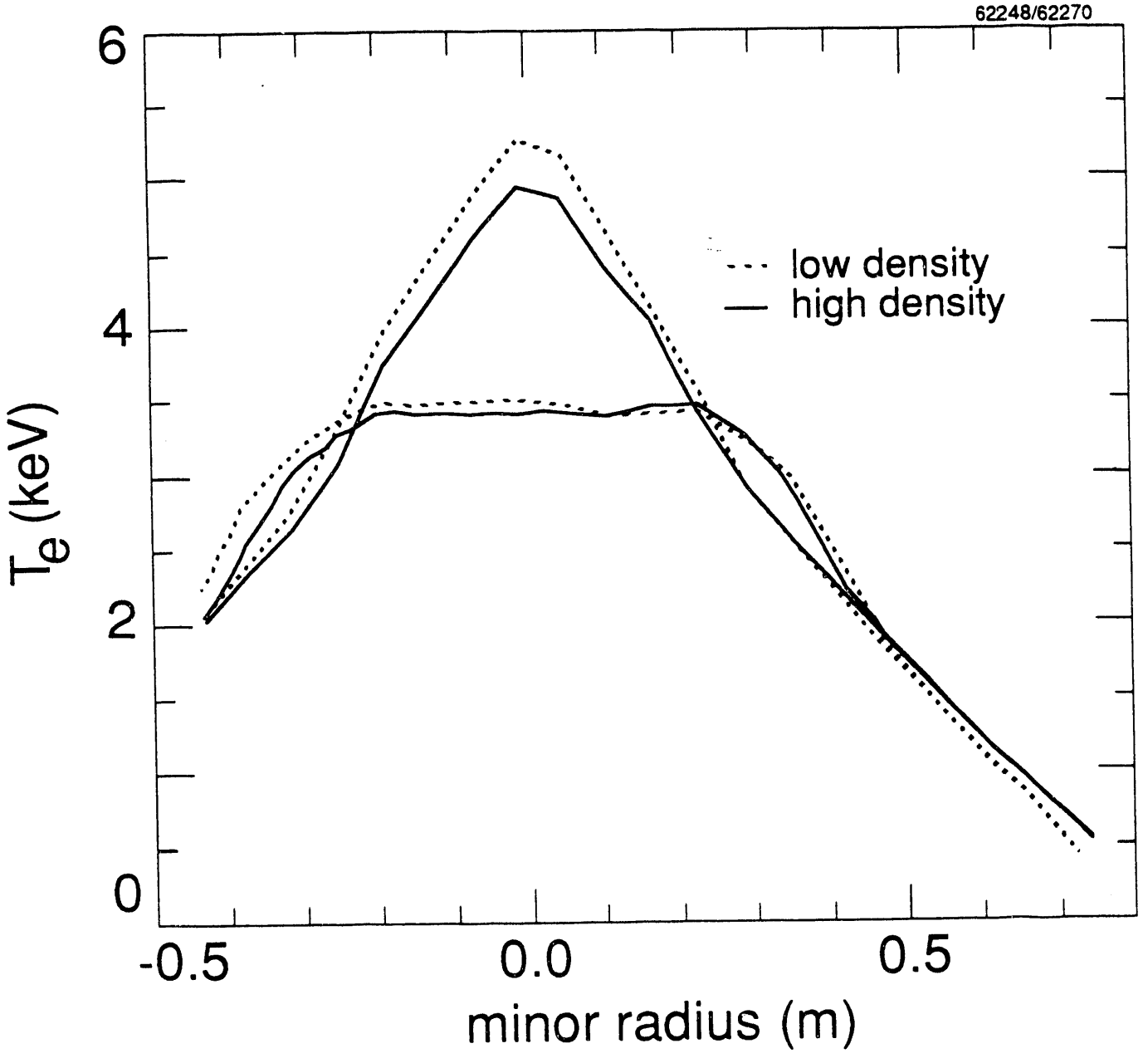
62248/62270
6
4
2
0
T_e (keV)
low density
high density
-0.5
0.0
0.5
minor radius (m)

Figure 4a

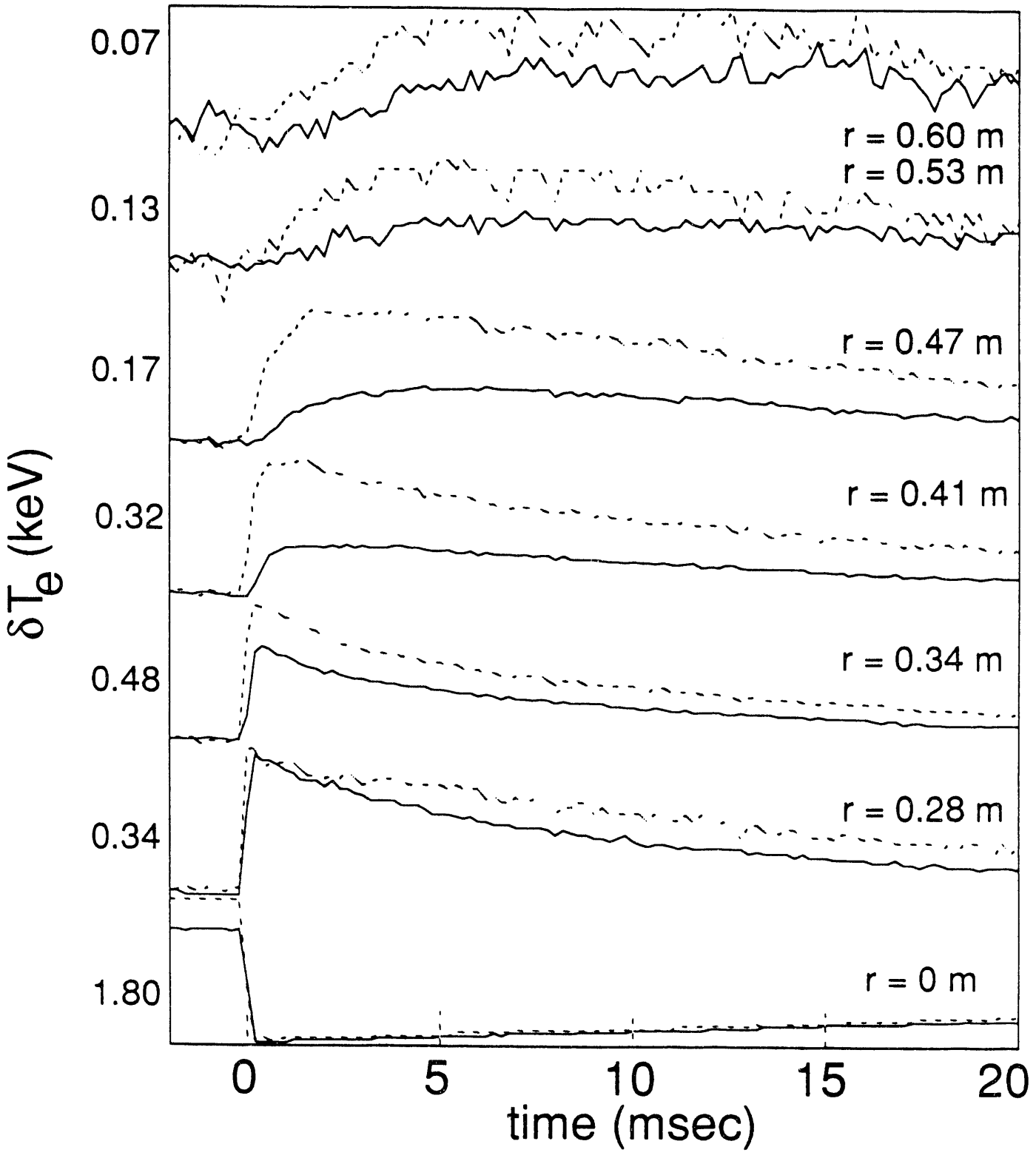

Figure 4b

62243_6 62270_2

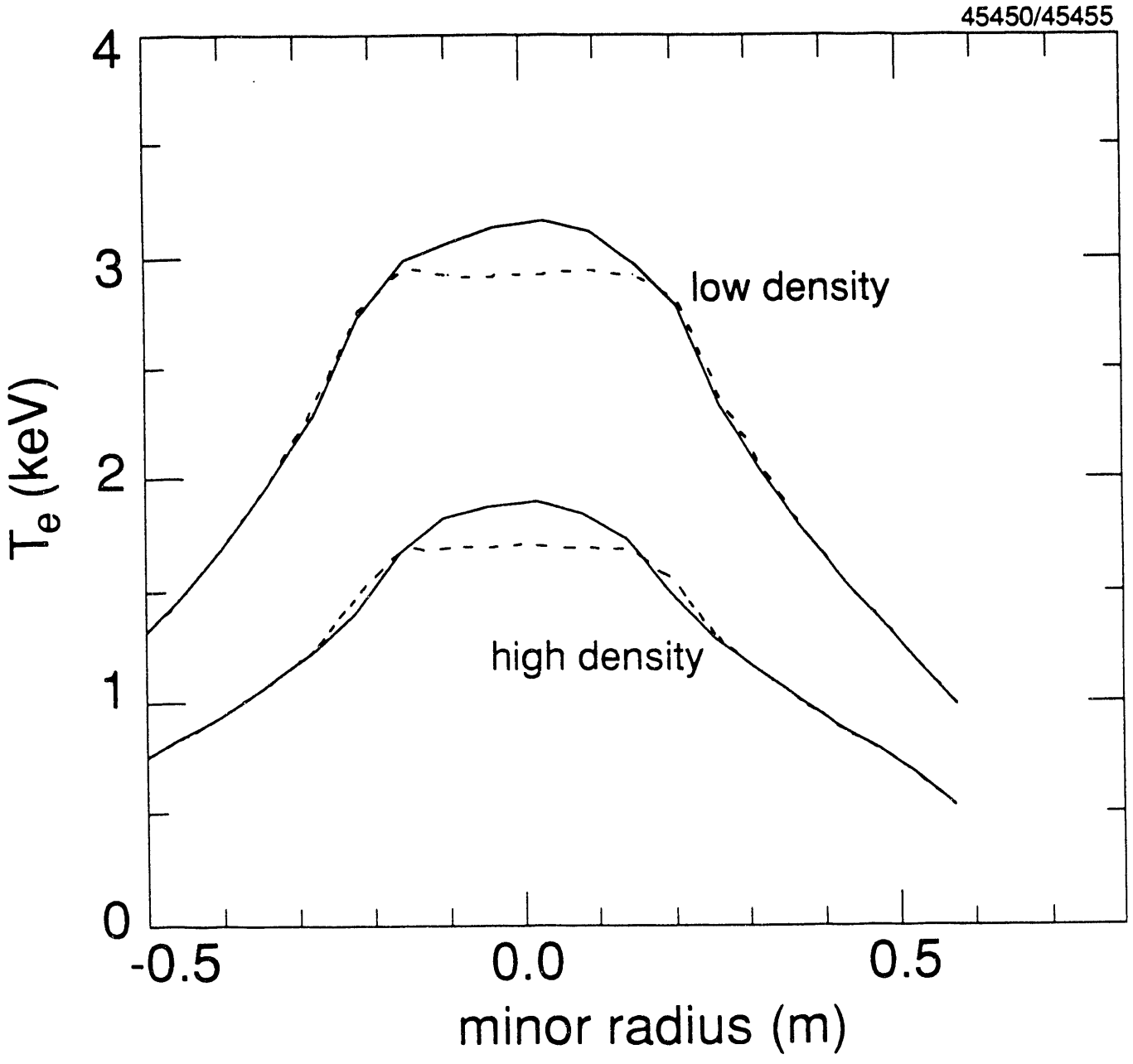
45450/45455
4
3
2
1
0
T_e (keV)
low density
high density
-0.5
0.0
0.5
minor radius (m)

Figure 5a

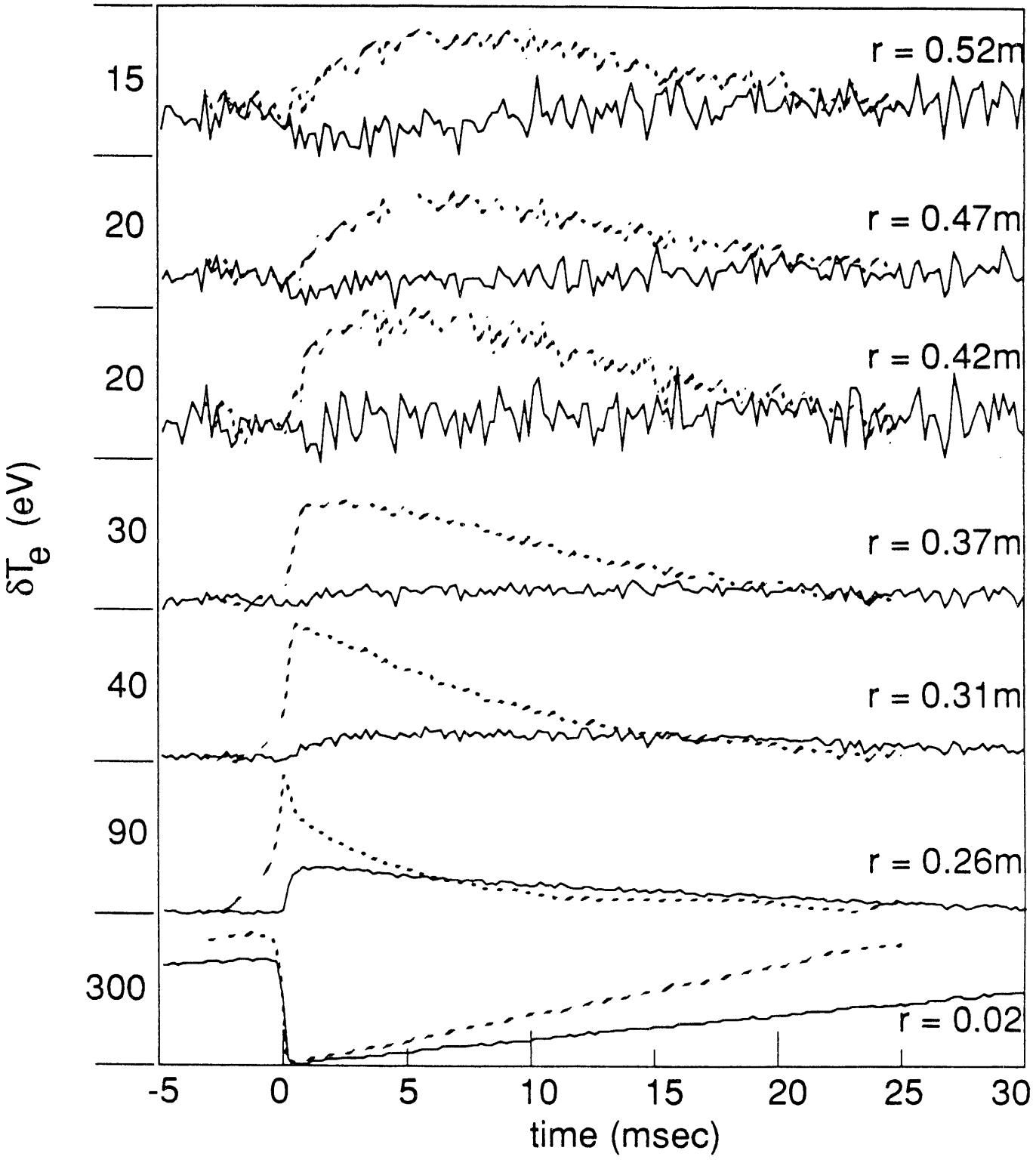
r = 0.52m
r = 0.47m
r = 0.42m
r = 0.37m
r = 0.31m
r = 0.26m
r = 0.02
15
20
20
30
40
90
300
δTe (eV)
-5
0
5
10
15
20
25
30
time (msec)

Figure 5b

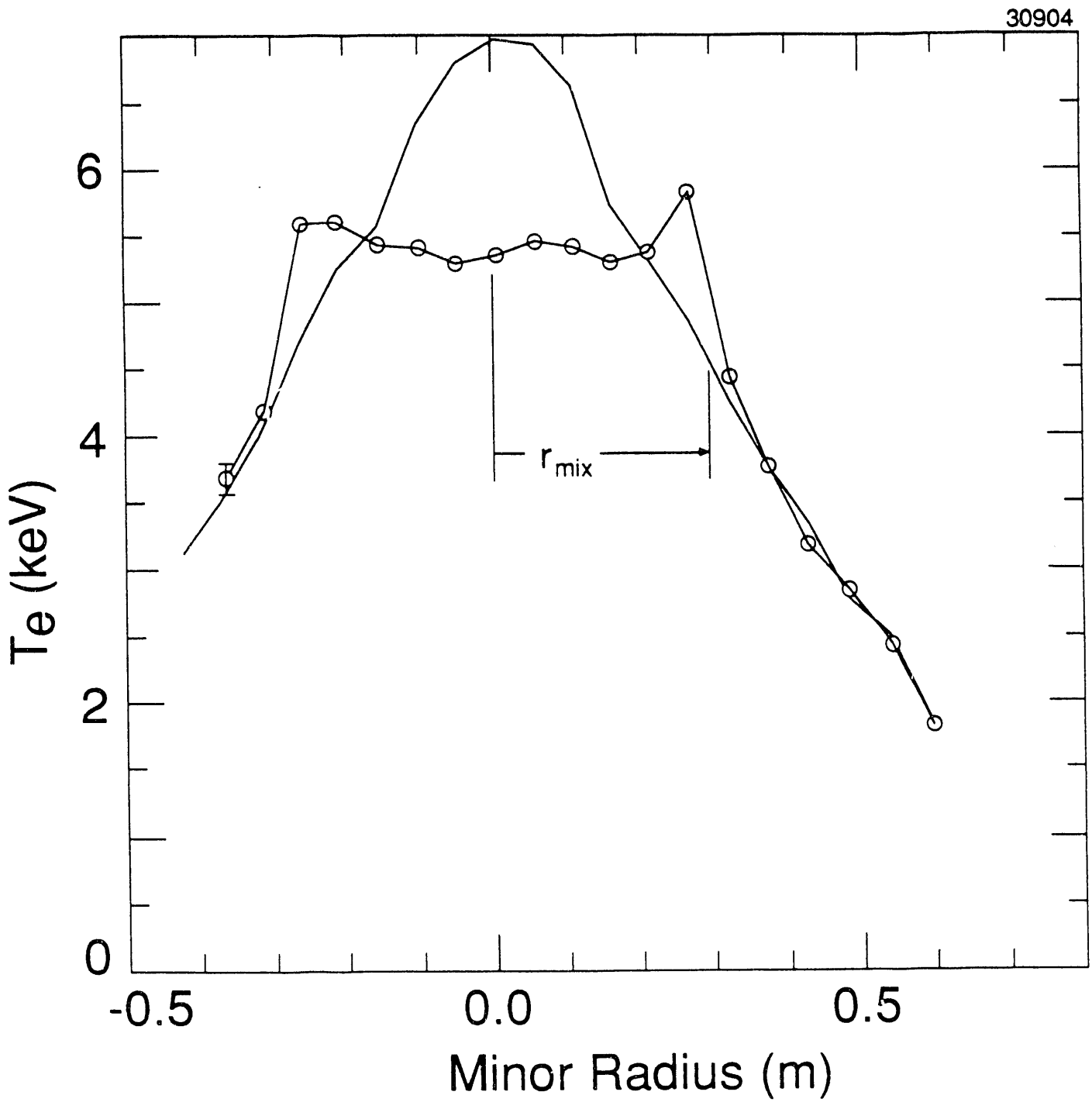

Figure 6

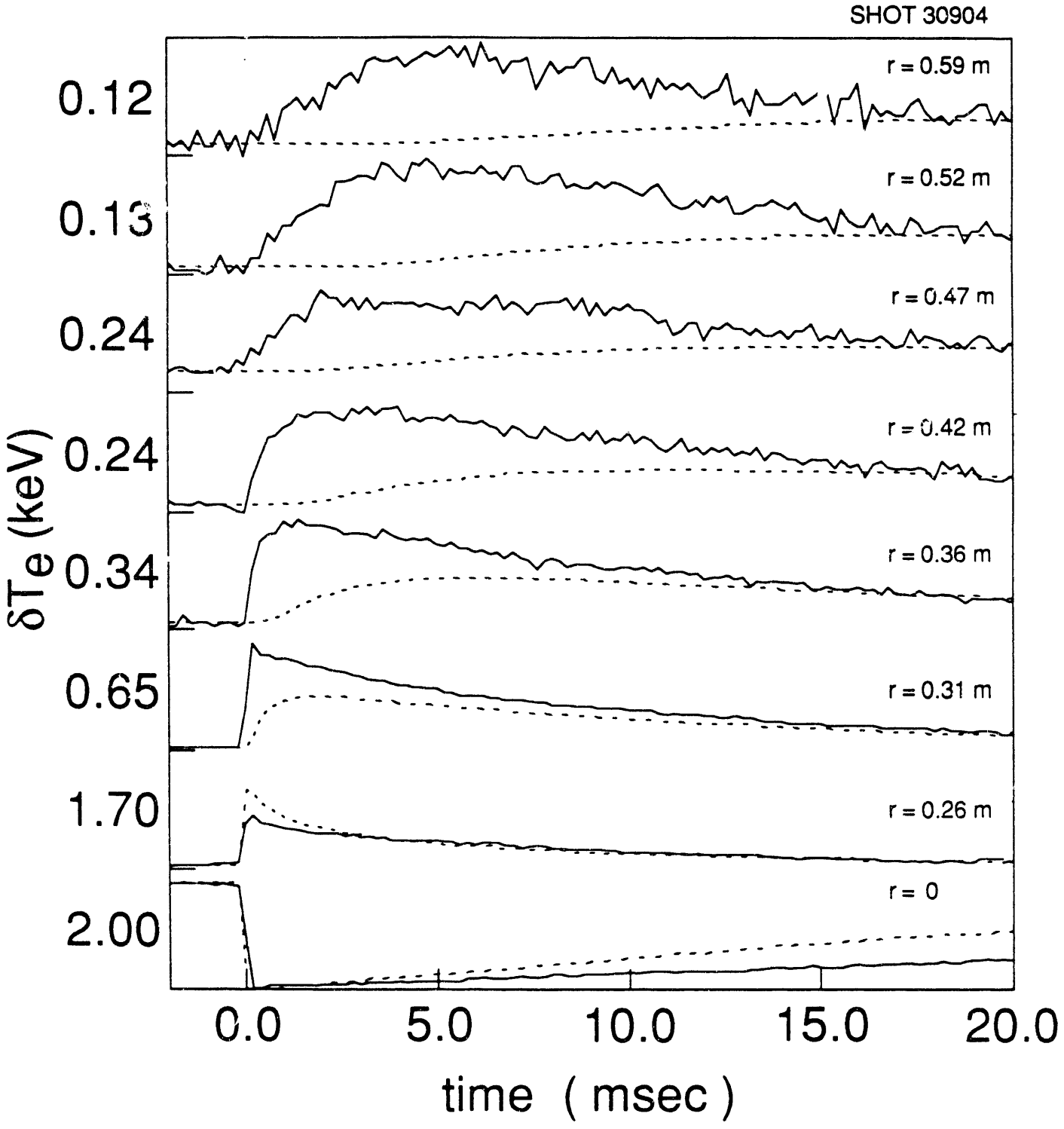
SHOT 30904
r = 0.59 m
r = 0.52 m
r = 0.47 m
r = 0.42 m
r = 0.36 m
r = 0.31 m
r = 0.26 m
r = 0
0.12
0.13
0.24
0.24
0.34
0.65
1.70
2.00
δTe (keV)
0.0
5.0
10.0
15.0
20.0
time (msec)

Figure 7

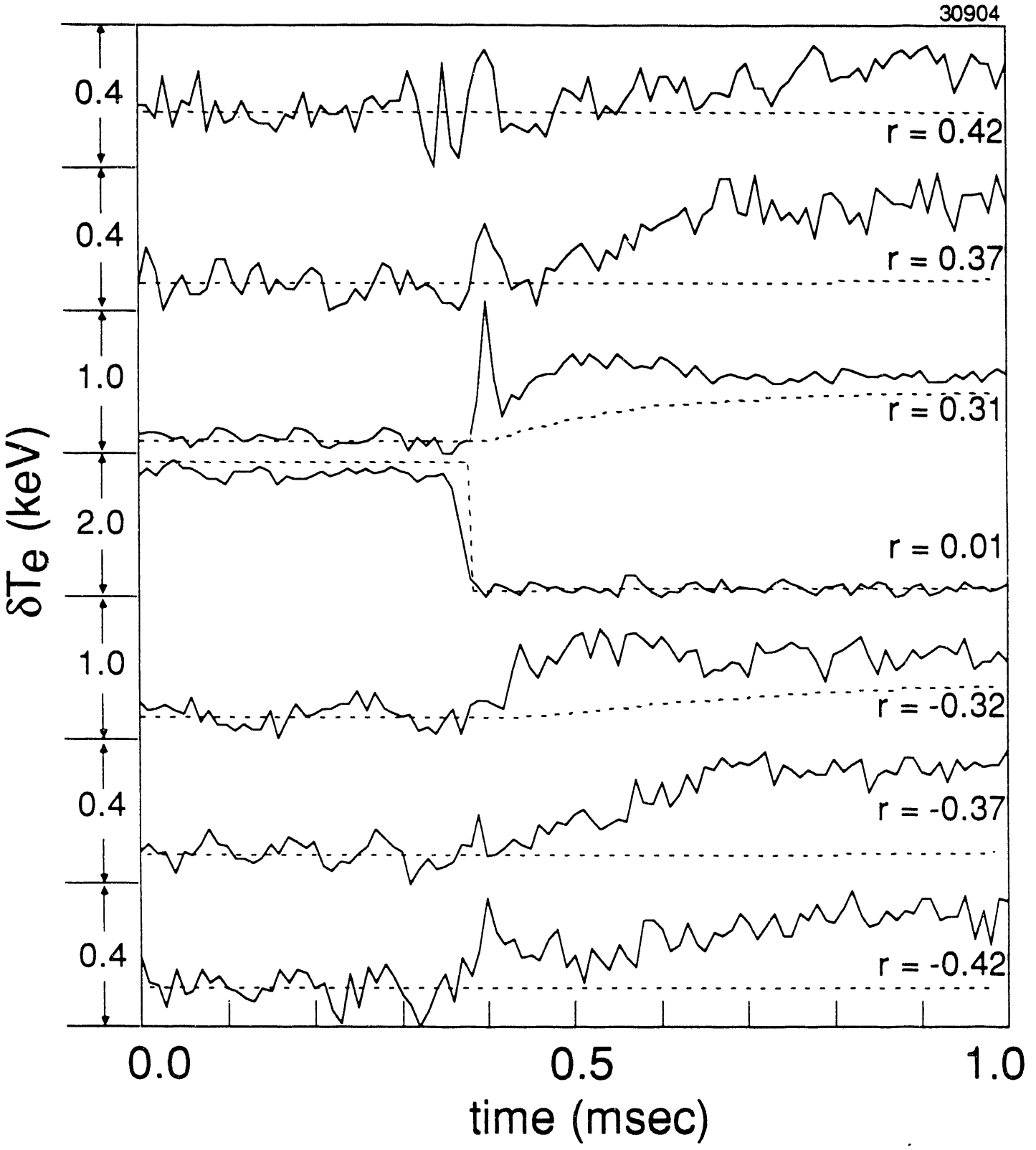
30904
0.4
0.4
1.0
2.0
1.0
0.4
0.4
r = 0.42
r = 0.37
r = 0.31
r = 0.01
r = -0.32
r = -0.37
r = -0.42
δTe (keV)
0.0
0.5
1.0
time (msec)

Figure 8

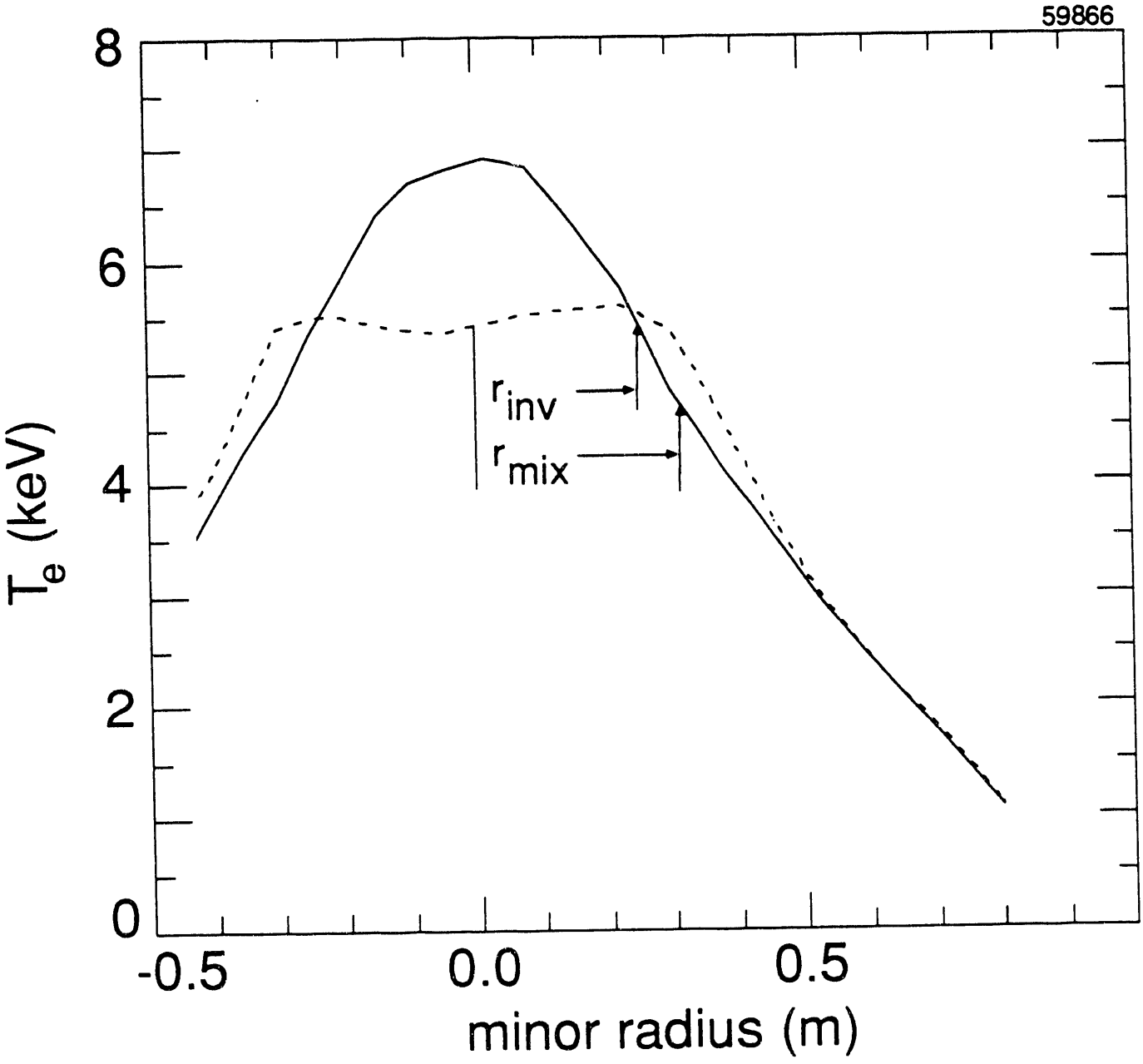

Figure 9

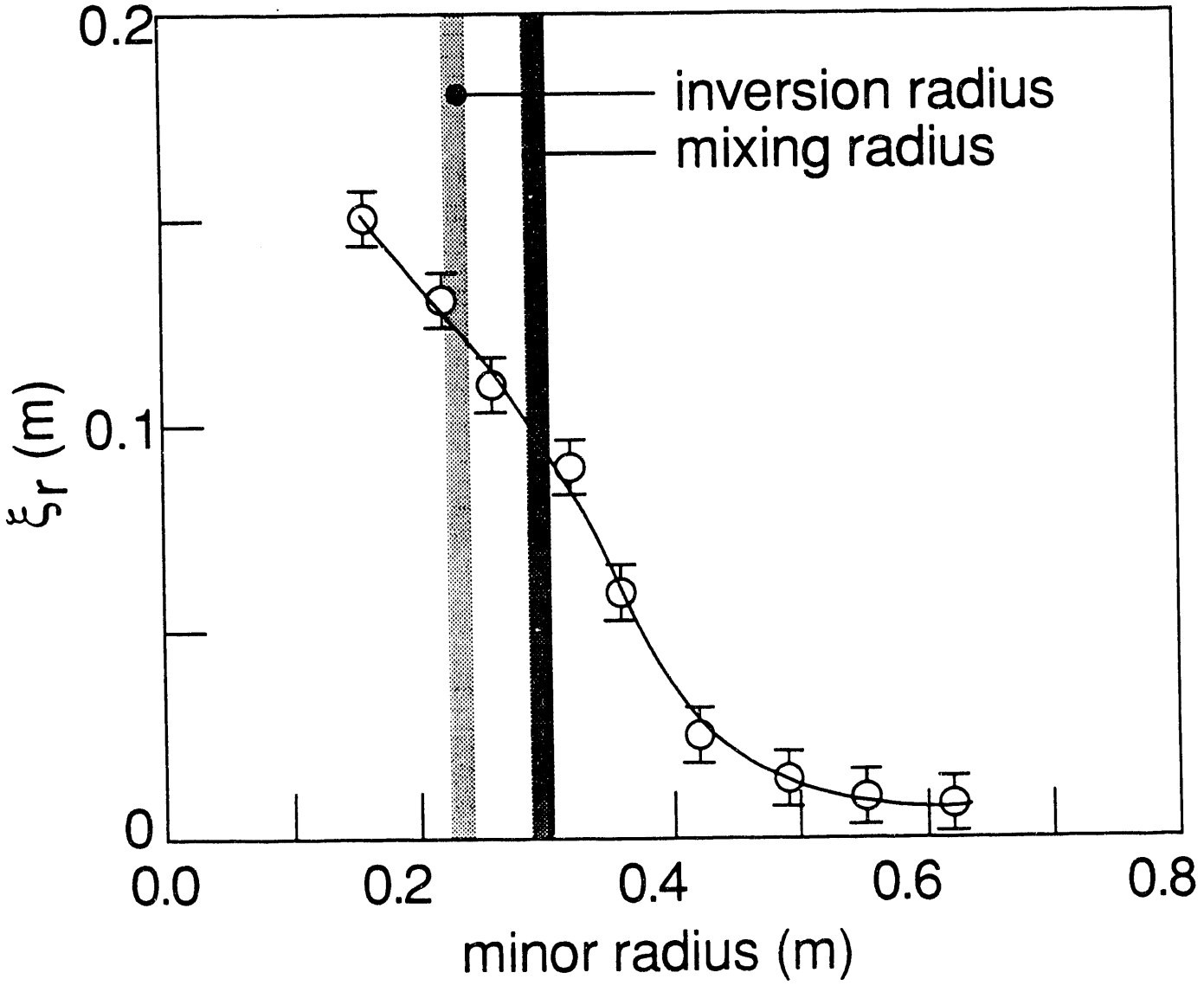
0.2
0.1
0
ξ_r (m)
inversion radius
mixing radius
0.0
0.2
0.4
0.6
0.8
minor radius (m)

Figure 10

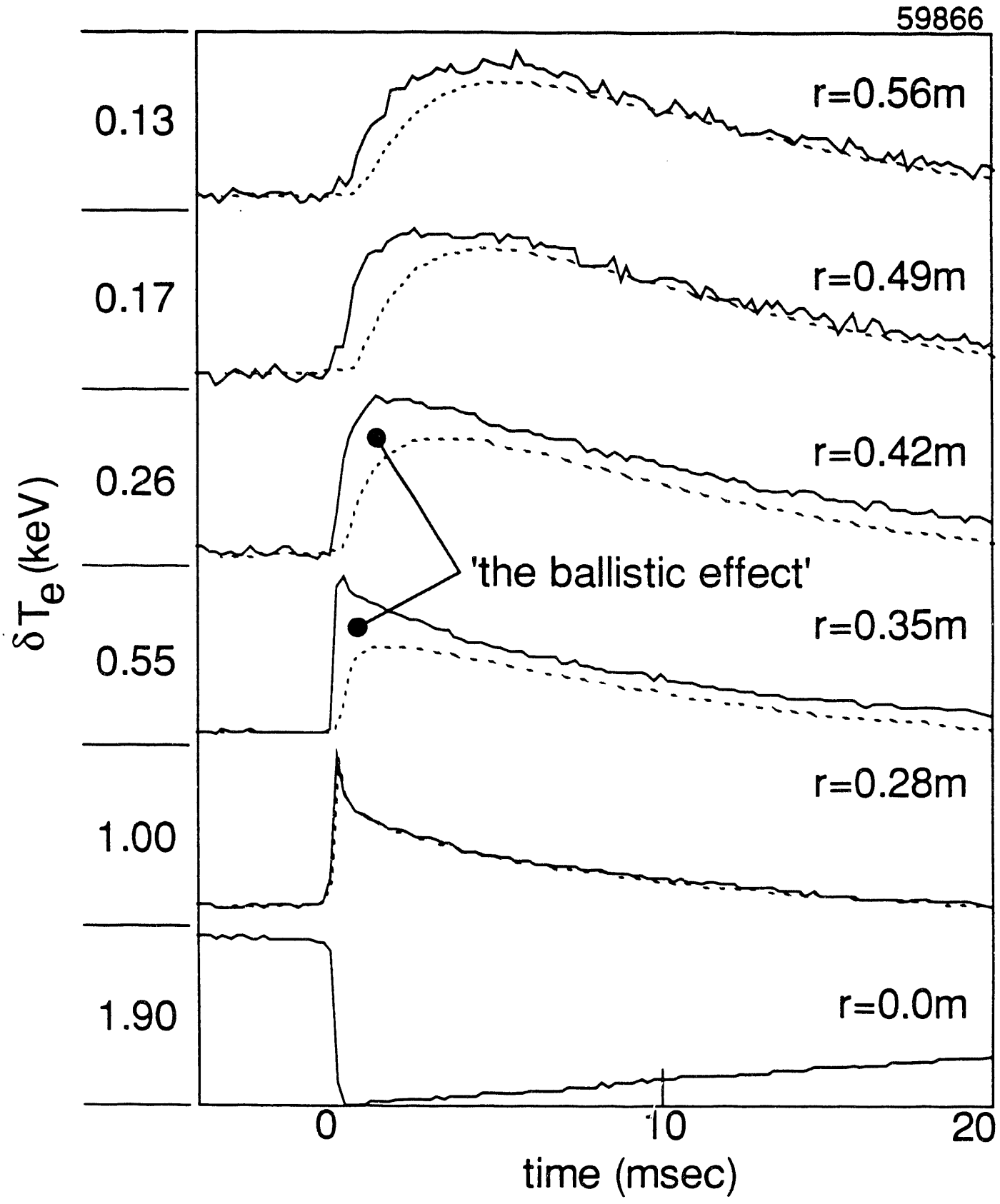
59866
0.13
0.17
0.26
0.55
1.00
1.90
r=0.56m
r=0.49m
r=0.42m
r=0.35m
r=0.28m
r=0.0m
'the ballistic effect'
δTe (keV)
0
10
20
time (msec)

Figure 11a

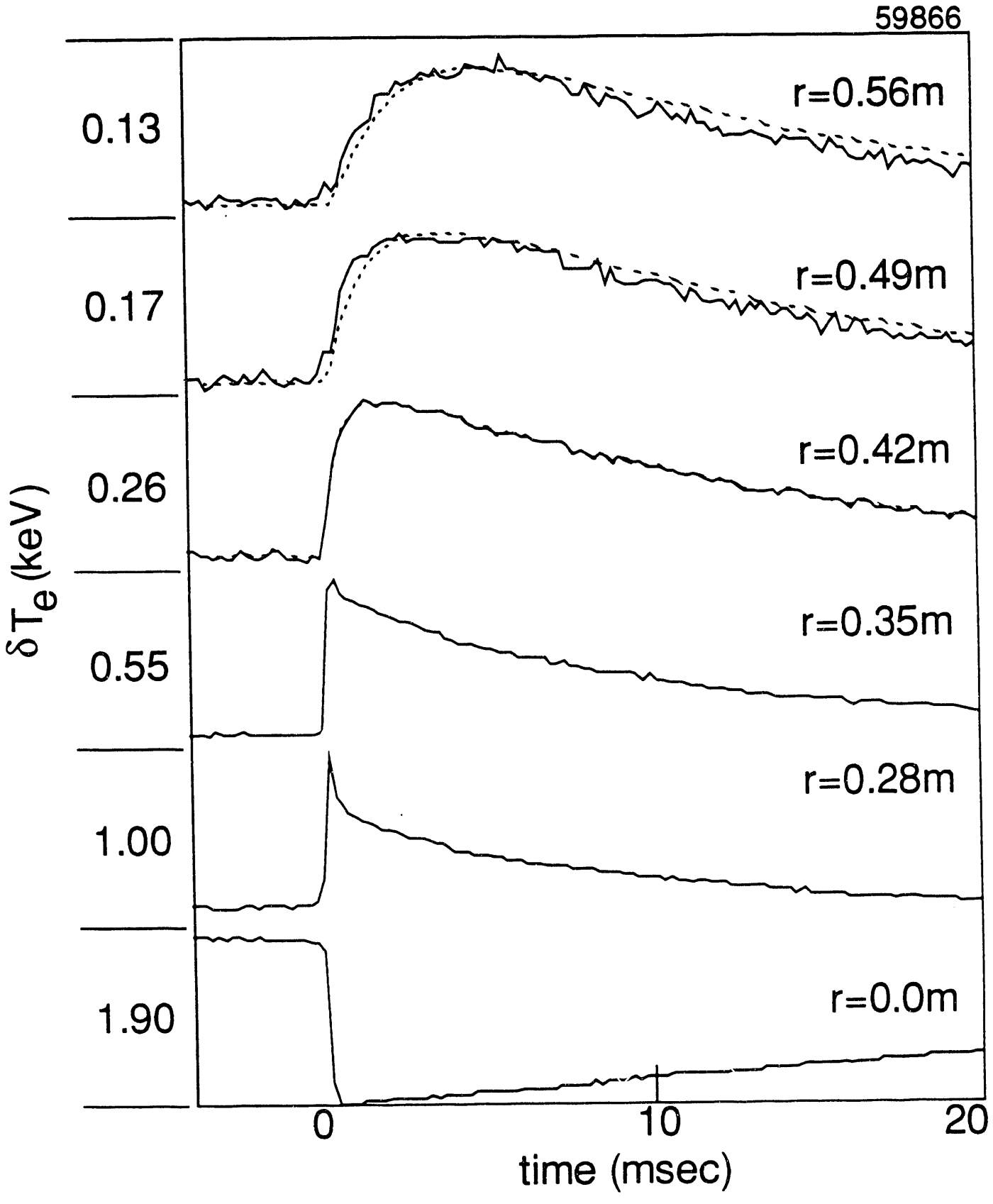
59866
r=0.56m
r=0.49m
r=0.42m
r=0.35m
r=0.28m
r=0.0m
0.13
0.17
0.26
0.55
1.00
1.90
δTe (keV)
0
10
20
time (msec)

Figure 11b

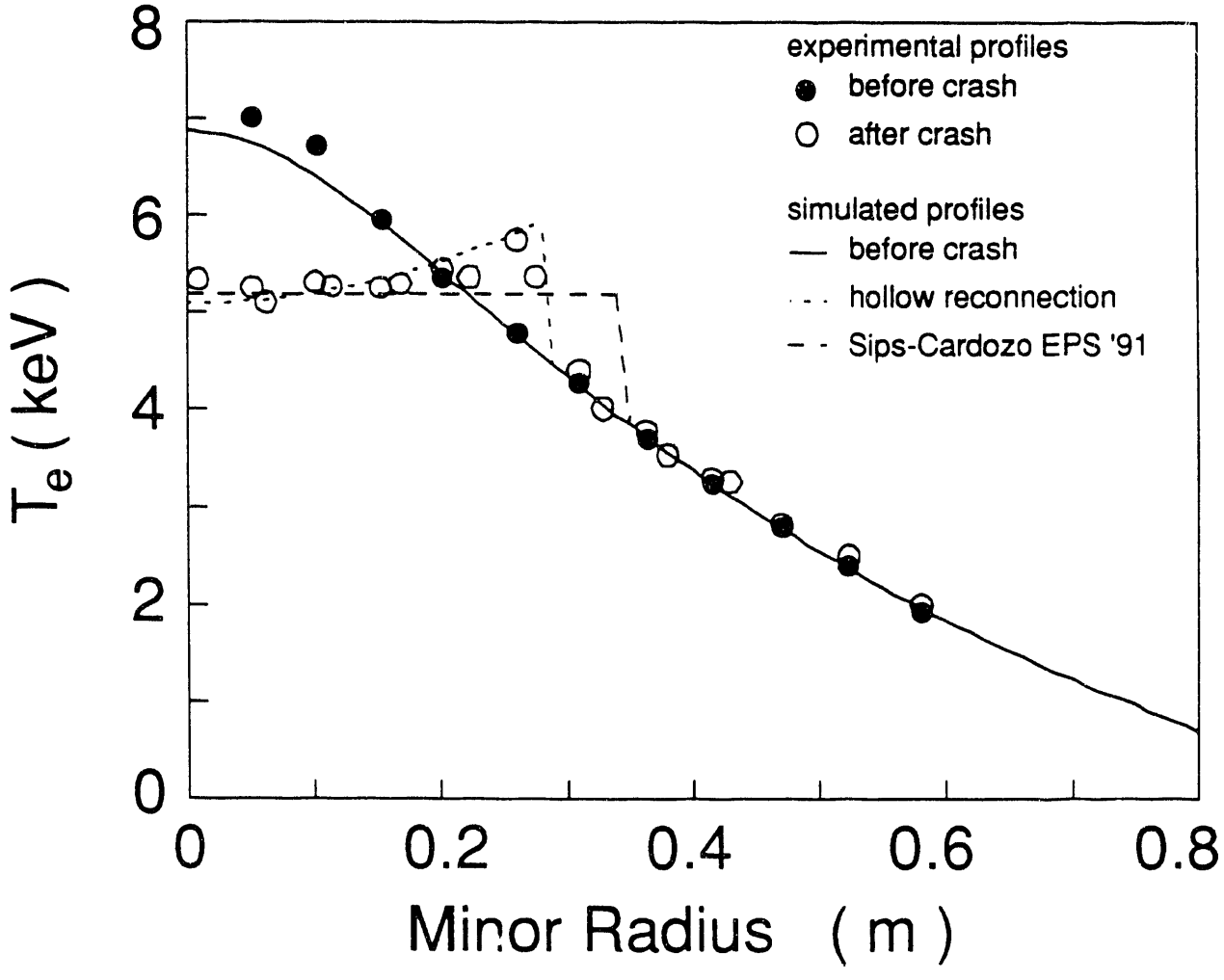
experimental profiles
before crash
after crash
simulated profiles
before crash
hollow reconnection
Sips-Cardozo EPS '91
T_e (keV)
Minor Radius (m)
0
2
4
6
8
0
0.2
0.4
0.6
0.8

Figure 12

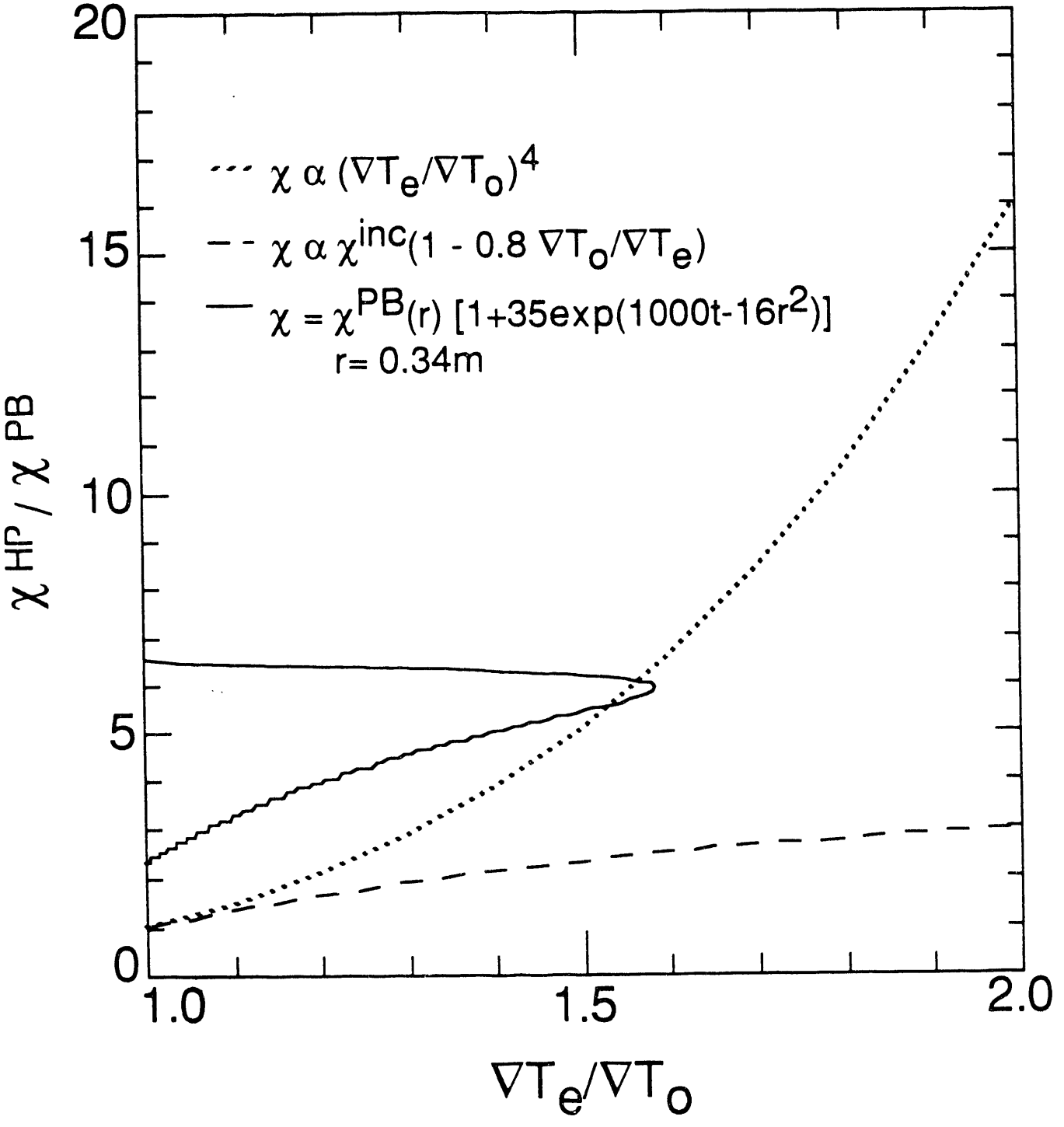
20
15
10
5
0
1.0
1.5
2.0
$\chi \alpha (\nabla T_e/\nabla T_o)^4$
$\chi \alpha \chi^{inc}(1 - 0.8\ \nabla T_o/\nabla T_e)$
$\chi = \chi^{PB}(r)\ [1+35\exp(1000t-16r^2)]$
r= 0.34m
χ^{HP}/χ^{PB}
$\nabla T_e/\nabla T_o$

Figure 13

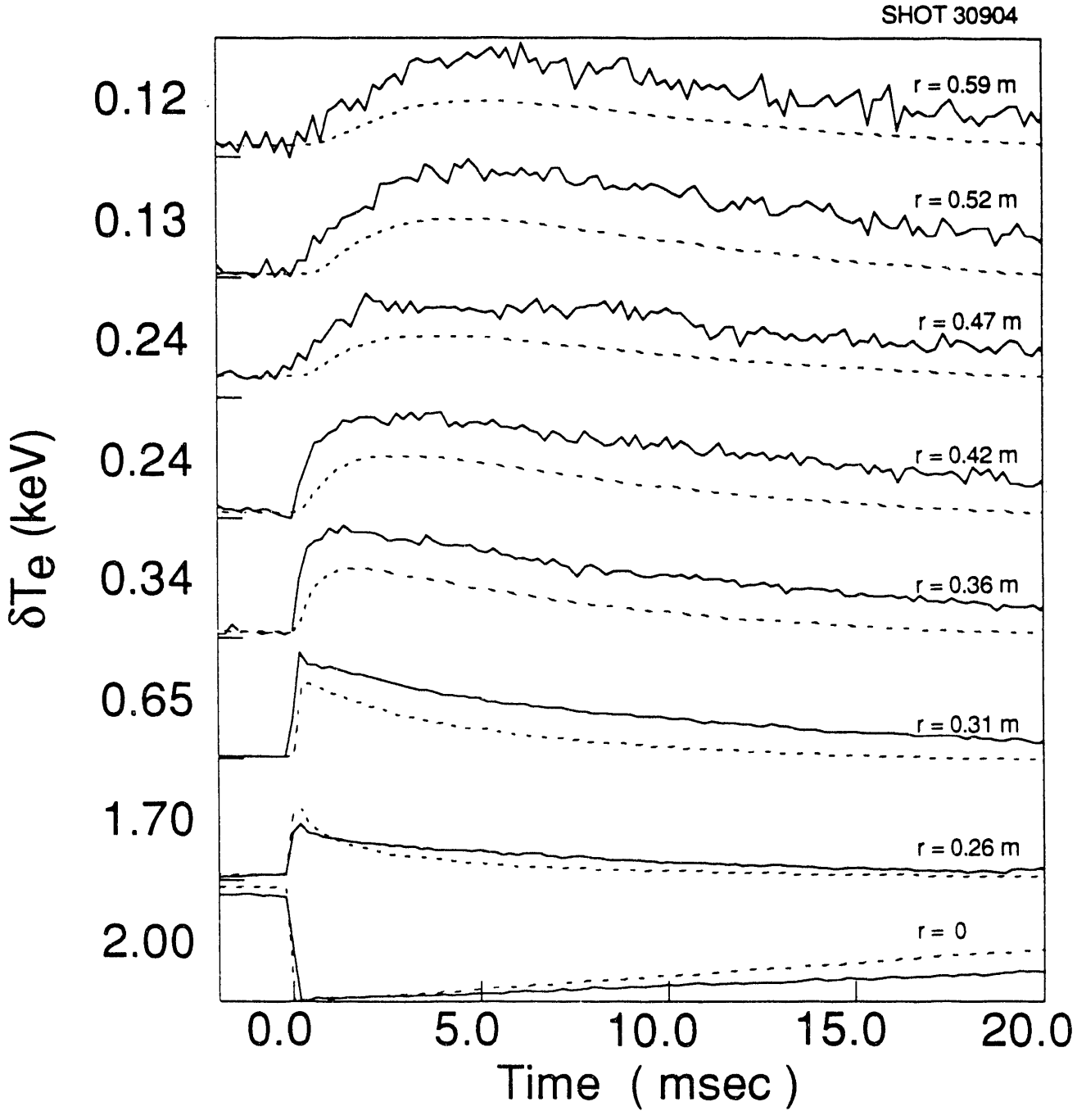
SHOT 30904
0.12
0.13
0.24
0.24
0.34
0.65
1.70
2.00
δTe (keV)
r = 0.59 m
r = 0.52 m
r = 0.47 m
r = 0.42 m
r = 0.36 m
r = 0.31 m
r = 0.26 m
r = 0
0.0
5.0
10.0
15.0
20.0
Time (msec)

Figure 14

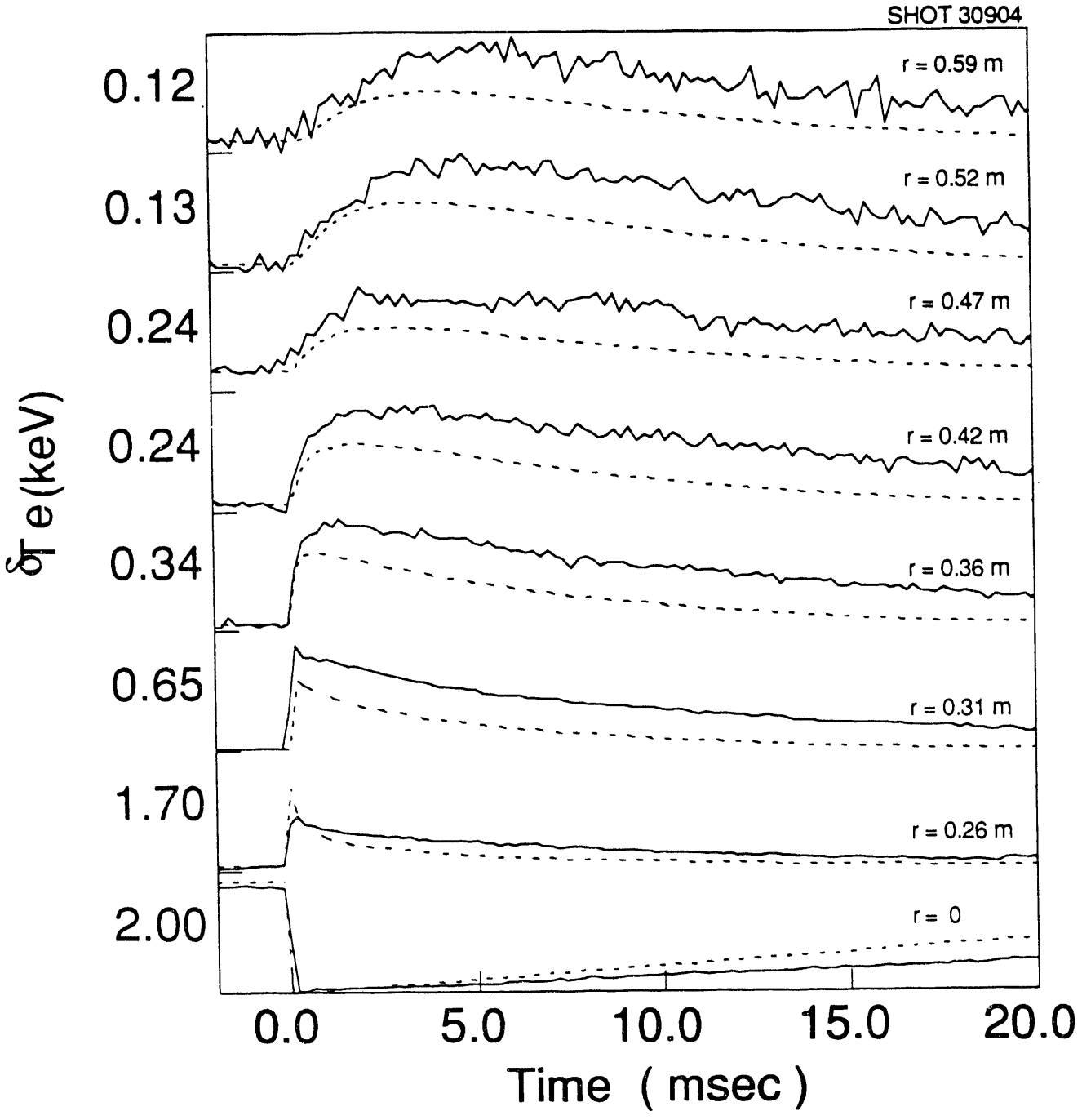
SHOT 30904
r = 0.59 m
r = 0.52 m
r = 0.47 m
r = 0.42 m
r = 0.36 m
r = 0.31 m
r = 0.26 m
r = 0
0.12
0.13
0.24
0.24
0.34
0.65
1.70
2.00
δTe(keV)
0.0
5.0
10.0
15.0
20.0
Time (msec)

Figure 15

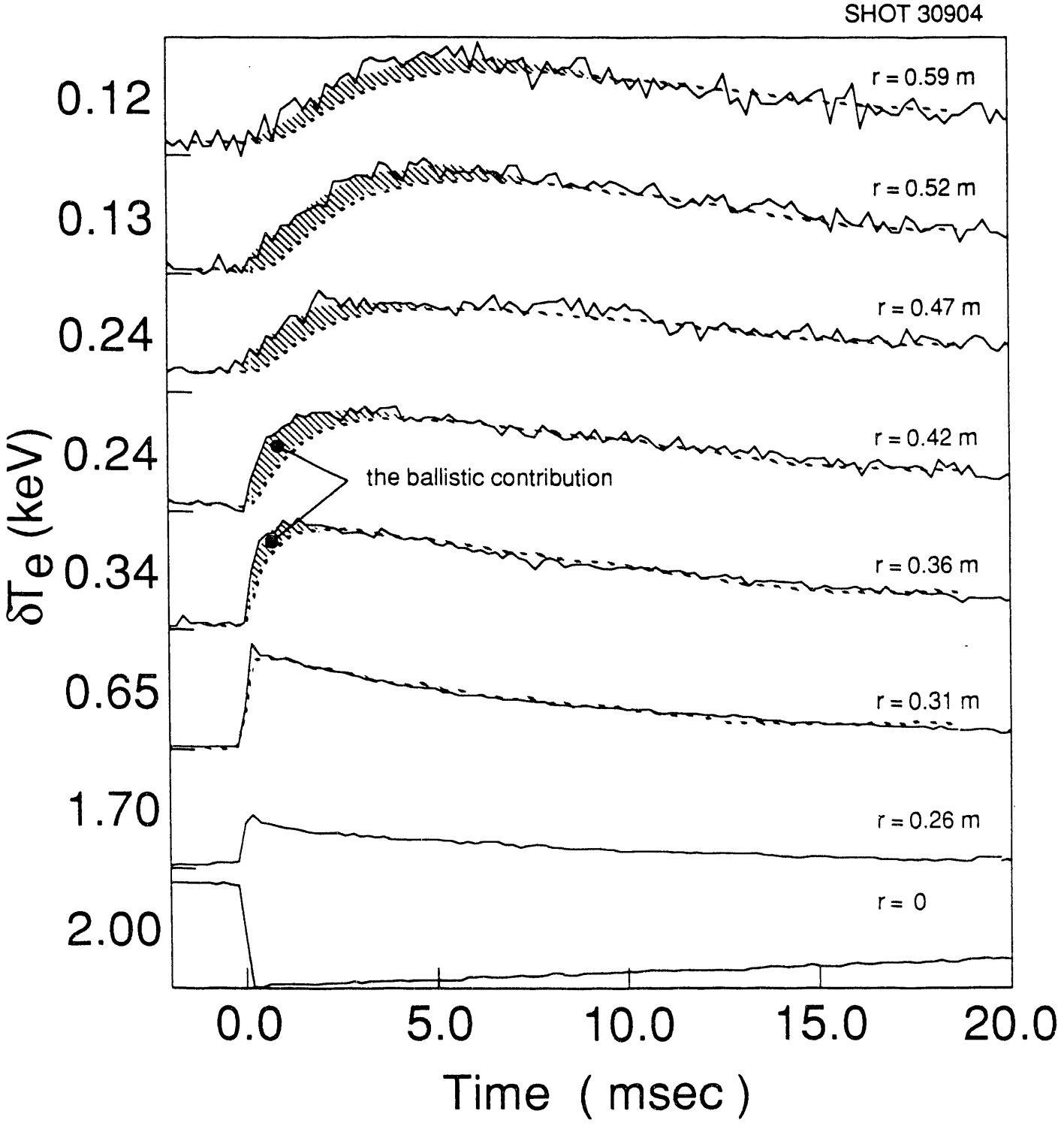
SHOT 30904
r = 0.59 m
r = 0.52 m
r = 0.47 m
r = 0.42 m
r = 0.36 m
r = 0.31 m
r = 0.26 m
r = 0
the ballistic contribution
0.12
0.13
0.24
0.24
0.34
0.65
1.70
2.00
δTe (keV)
0.0
5.0
10.0
15.0
20.0
Time (msec)

Figure 16a

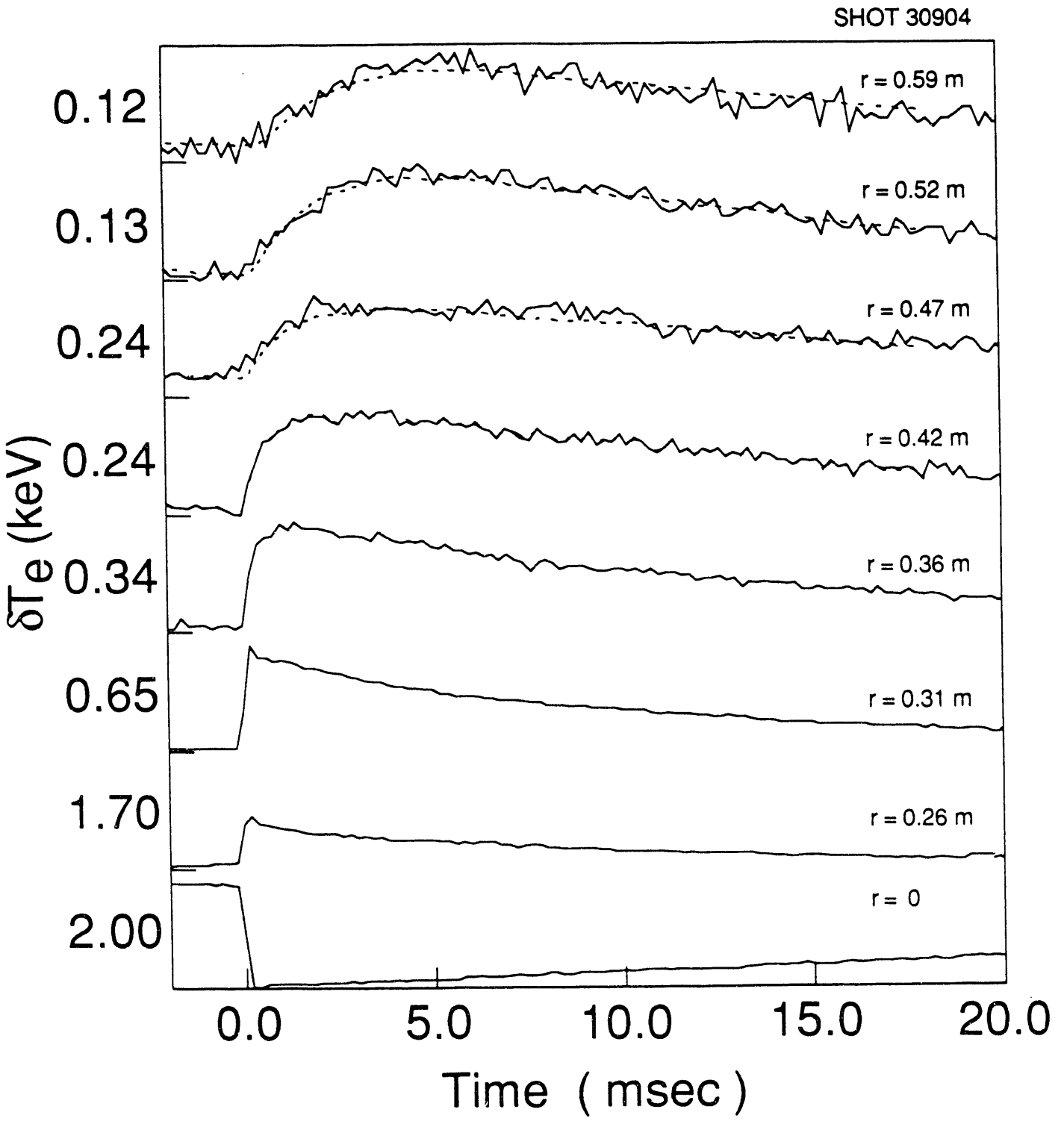
SHOT 30904
r = 0.59 m
r = 0.52 m
r = 0.47 m
r = 0.42 m
r = 0.36 m
r = 0.31 m
r = 0.26 m
r = 0
0.12
0.13
0.24
0.24
0.34
0.65
1.70
2.00
δTe (keV)
0.0
5.0
10.0
15.0
20.0
Time (msec)

Figure 16b

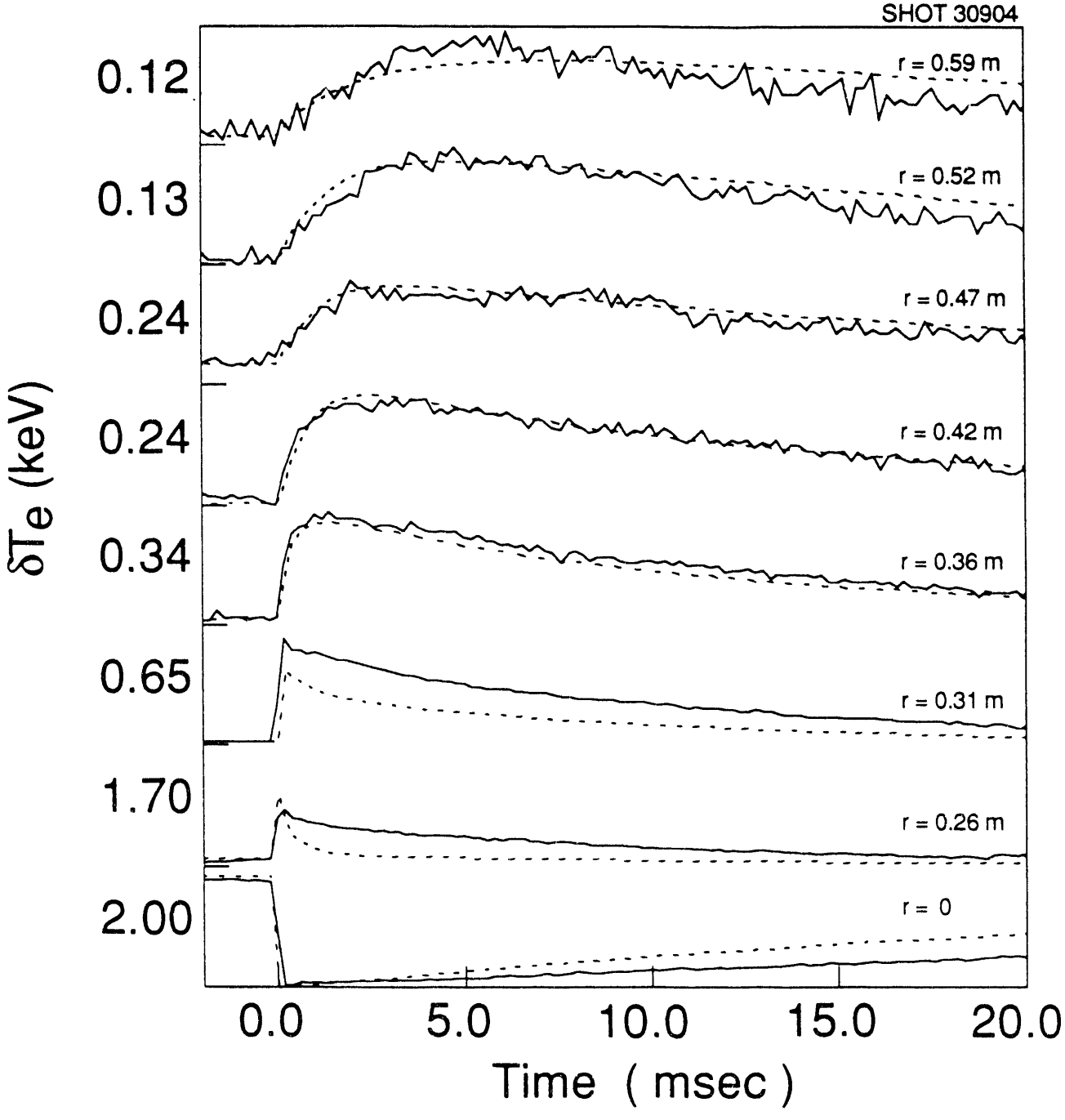
SHOT 30904
r = 0.59 m
r = 0.52 m
r = 0.47 m
r = 0.42 m
r = 0.36 m
r = 0.31 m
r = 0.26 m
r = 0
0.12
0.13
0.24
0.24
0.34
0.65
1.70
2.00
δTe (keV)
0.0
5.0
10.0
15.0
20.0
Time (msec)

Figure 17

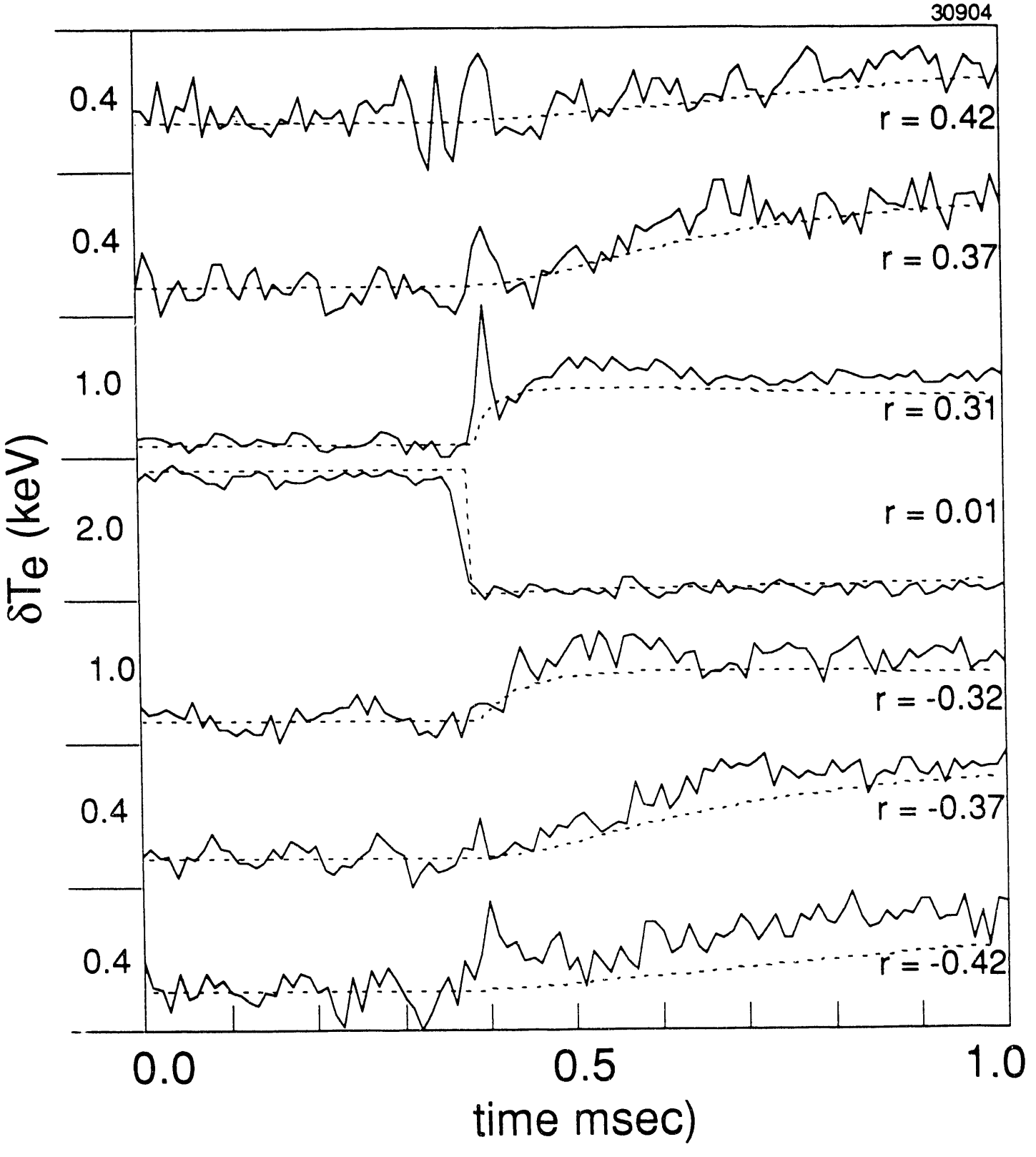
30904
0.4
r = 0.42
0.4
r = 0.37
1.0
r = 0.31
2.0
r = 0.01
1.0
r = -0.32
0.4
r = -0.37
0.4
r = -0.42
δTe (keV)
0.0
0.5
1.0
time msec)

Figure 18

EXTERNAL DISTRIBUTION IN ADDITION TO UC-420

Dr. F. Paoloni, Univ. of Wollongong, AUSTRALIA
Prof. M.H. Brennan, Univ. of Sydney, AUSTRALIA
Plasma Research Lab., Australian Nat. Univ., AUSTRALIA
Prof. I.R. Jones, Flinders Univ, AUSTRALIA
Prof. F. Cap, Inst. for Theoretical Physics, AUSTRIA
Prof. M. Heindler, Institut für Theoretische Physik, AUSTRIA
Prof. M. Goossens, Astronomisch Instituut, BELGIUM
Ecole Royale Militaire, Lab. de Phy. Plasmas, BELGIUM
Commission-European, DG. XII-Fusion Prog., BELGIUM
Prof. R. Boucique, Rijksuniversiteit Gent, BELGIUM
Dr. P.H. Sakanaka, Instituto Fisica, BRAZIL
Instituto Nacional De Pesquisas Espaciais-INPE, BRAZIL
Documents Office, Atomic Energy of Canada Ltd., CANADA
Dr. M.P. Bachynski, MPB Technologies, Inc., CANADA
Dr. H.M. Skarsgard, Univ. of Saskatchewan, CANADA
Prof. J. Teichmann, Univ. of Montreal, CANADA
Prof. S.R. Sreenivasan, Univ. of Calgary, CANADA
Prof. T.W. Johnston, INRS-Energie, CANADA
Dr. R. Bolton, Centre canadien de fusion magnétique, CANADA
Dr. C.R. James,, Univ. of Alberta, CANADA
Dr. P. Lukác, Komenského Universzita, CZECHO-SLOVAKIA
The Librarian, Culham Laboratory, ENGLAND
Library, R61, Rutherford Appleton Laboratory, ENGLAND
Mrs. S.A. Hutchinson, JET Library, ENGLAND
Dr. S.C. Sharma, Univ. of South Pacific, FIJI ISLANDS
P. Mähönen, Univ. of Helsinki, FINLAND
Prof. M.N. Bussac, Ecole Polytechnique,, FRANCE
C. Mouttet, Lab. de Physique des Milieux Ionisés, FRANCE
J. Radet, CEN/CADARACHE - Bat 506, FRANCE
Prof. E. Economou, Univ. of Crete, GREECE
Ms. C. Rinni, Univ. of Ioannina, GREECE
Dr. T. Mual, Academy Bibliographic Ser., HONG KONG
Preprint Library, Hungarian Academy of Sci., HUNGARY
Dr. B. DasGupta, Saha Inst. of Nuclear Physics, INDIA
Dr. P. Kaw, Inst. for Plasma Research, INDIA
Dr. P. Rosenau, Israel Inst. of Technology, ISRAEL
Librarian, International Center for Theo. Physics, ITALY
Miss C. De Palo, Associazione EURATOM-ENEA, ITALY
Dr. G. Grosso, Istituto di Fisica del Plasma, ITALY
Prof. G. Rostangni, Istituto Gas Ionizzati Del Cnr, ITALY
Dr. H. Yamato, Toshiba Res. & Devel. Center, JAPAN
Prof. I. Kawakami, Hiroshima Univ., JAPAN
Prof. K. Nishikawa, Hiroshima Univ., JAPAN
Director, Japan Atomic Energy Research Inst., JAPAN
Prof. S. Itoh, Kyushu Univ., JAPAN
Research Info. Ctr., National Instit. for Fusion Science, JAPAN
Prof. S. Tanaka, Kyoto Univ., JAPAN
Library, Kyoto Univ., JAPAN
Prof. N. Inoue, Univ. of Tokyo, JAPAN
Secretary, Plasma Section, Electrotechnical Lab., JAPAN
S. Mori, Technical Advisor, JAERI, JAPAN
Dr. O. Mitarai, Kumamoto Inst. of Technology, JAPAN
J. Hyeon-Sook, Korea Atomic Energy Research Inst., KOREA
D.I. Choi, The Korea Adv. Inst. of Sci. & Tech., KOREA
Prof. B.S. Liley, Univ. of Waikato, NEW ZEALAND
Inst of Physics, Chinese Acad Sci PEOPLE'S REP. OF CHINA
Library, Inst. of Plasma Physics, PEOPLE'S REP. OF CHINA
Tsinghua Univ. Library, PEOPLE'S REPUBLIC OF CHINA
Z. Li, S.W. Inst. Physics, PEOPLE'S REPUBLIC OF CHINA
Prof. J.A.C. Cabral, Instituto Superior Tecnico, PORTUGAL
Dr. O. Petrus, ALI CUZA Univ., ROMANIA
Dr. J. de Villiers, Fusion Studies, AEC, S. AFRICA
Prof. M.A. Hellberg, Univ. of Natal, S. AFRICA
Prof. D.E. Kim, Pohang Inst. of Sci. & Tech., SO. KOREA
Prof. C.I.E.M.A.T, Fusion Division Library, SPAIN
Dr. L. Stenflo, Univ. of UMEA, SWEDEN
Library, Royal Inst. of Technology, SWEDEN
Prof. H. Wilhelmson, Chalmers Univ. of Tech., SWEDEN
Centre Phys. Des Plasmas, Ecole Polytech, SWITZERLAND
Bibliotheek, Inst. Voor Plasma-Fysica, THE NETHERLANDS
Asst. Prof. Dr. S. Cakir, Middle East Tech. Univ., TURKEY
Dr. V.A. Glukhikh, Sci. Res. Inst. Electrophys.I Apparatus, USSR
Dr. D.D. Ryutov, Siberian Branch of Academy of Sci., USSR
Dr. G.A. Eliseev, I.V. Kurchatov Inst., USSR
Librarian, The Ukr.SSR Academy of Sciences, USSR
Dr. L.M. Kovrizhnykh, Inst. of General Physics, USSR
Kernforschungsanlage GmbH, Zentralbibliothek, W. GERMANY
Bibliothek, Inst. Für Plasmaforschung, W. GERMANY
Prof. K. Schindler, Ruhr-Universität Bochum, W. GERMANY
Dr. F. Wagner, (ASDEX), Max-Planck-Institut, W. GERMANY
Librarian, Max-Planck-Institut, W. GERMANY
Prof. R.K. Janev, Inst. of Physics, YUGOSLAVIA

DATE
FILMED
10/20/93

END